Atmos. Chem. Phys., 26, 16719–16739, 2026
https://doi.org/10.5194/acp-26-16719-2026
© Author(s) 2026. This work is distributed under
the Creative Commons Attribution 4.0 License.

Atmospheric Chemistry and Physics Open Access

Research article

Marine organic aerosols reflect ecosystem variability from phytoplankton functional types to micronekton

Emmanuel Chevassus[1], Vaios Moschos[1], Kirsten N. Fossum[1], Lu Lei[1], Liz Coleman[1], Dagmar B. Stengel[1], David Nganga[1], Vignesh Prabhu[1], Wei Xu[1,a], Darius Ceburnis[1], Colin O'Dowd[1], and Jurgita Ovadnevaite[1]

[1]School of Natural Sciences, Ryan Institute's Centre for Climate and Air Pollution Studies, University of Galway, H91 TK33, Co. Galway, Ireland
[a]now at: Institute of Urban Environment, Chinese Academy of Sciences, Xiamen 361021, China

Correspondence: Jurgita Ovadnevaite (jurgita.ovadnevaite@universityofgalway.ie)

Received: 13 May 2026 – Discussion started: 27 May 2026
Revised: 14 October 2026 – Accepted: 15 November 2026 – Published: 23 November 2026

Abstract. Marine organic aerosols remain a major source of uncertainty in aerosol cloud-climate interactions, in part because marine ecosystem structure and biological drivers are typically reduced to bulk chlorophyll-*a*. Here, a full year of high-resolution aerosol mass spectrometry measurements at Mace Head (west coast of Ireland) is combined with HYSPLIT air-masses exposure and gap-free phytoplankton functional type (PFT) fields to explore influences on primary marine organic aerosol (PMOA) and methanesulphonic acid (MSA). During the spring-summer diatom climax, PMOA correlates with dominant bloom taxa ($R = 0.62$–0.70) and micronekton ($R = 0.55$). Strong PFTs covariance, however, prevented robust attribution to a single species. Cross-entropy showed PMOA maxima at 0–2 d for bloom-forming taxa and micronekton at 14 d, consistent with early labile release and later lysis/grazing while MSA also showed lagged associations to both PFT and micronekton. Mechanical forcing was evaluated from source-region wave Reynolds number, whitecap coverage and bubble-plume penetration. Across the three selected case studies, PMOA reflected the balance between ecosystem state and air-sea transfer. Spring–summer 2018 case combined high sea-surface particulate organic carbon (POC) and nutrients drawdown with sufficient air-sea transfer; August 2018 had stronger forcing, but lower POC while August 2009 combined higher POC and the strongest air-sea transfer. These findings support considering ecosystem composition and nutrients alongside air-sea transfer when representing natural marine aerosols and motivate future research vessel campaigns and mesocosm experiments to explicitly manipulate PFT interactions.

1 Introduction

The Earth's energy imbalance has more than doubled in recent decades, driven primarily by anthropogenic greenhouse-gas emissions, with additional contributions from declining planetary albedo linked to sea-surface temperature changes and aerosol-cloud feedback (Mauritsen et al., 2025). Anthropogenic effective radiative forcing (RF) since 1750 is estimated at $2.72\,W\,m^{-2}$ [1.96 to $3.48\,W\,m^{-2}$] while aerosol-radiation interactions contribute $-0.22\,W\,m^{-2}$ [-0.47 to $0.04\,W\,m^{-2}$] and submicron aerosol-cloud indirect interactions $-0.84\,W\,m^{-2}$ [-1.45 to $-0.25\,W\,m^{-2}$], reflecting substantial uncertainties from aerosol-cloud interactions that remain poorly constrained in Intergovernmental Panel on Climate Change (IPCC) reports (Forster et al., 2023). Beyond these anthropogenic influences, growing evidence also suggest that natural marine sources play a larger role than previously thought in modulating global RF, emphasising the urgent need for improved observational and process-level understanding (Hodshire et al., 2019; Sellegri et al., 2024). Concurrently, climate change increasingly modifies ocean biogenic activity and air-sea transfer physics (Hong et al., 2025; Law and Miller, 2025), thereby altering the global pool of marine aerosols including sea salt, oxidised secondary or-

ganic aerosol, methanesulphonic acid (MSA), and primary marine organic aerosol (PMOA) that seed low-level marine clouds.

PMOA is produced by breaking waves as bubbles containing biogenic sea spray burst at the ocean's surface (O'Dowd et al., 2004; Ovadnevaite et al., 2014a; Villermaux et al., 2022). As a result of measurements and modelling propagating uncertainties, global PMOA fluxes are not yet fully resolved with estimates ranging from 9 to 29 Tg yr^{-1} (Burrows et al., 2022; Leon-Marcos et al., 2025) while global PMOA contribution to indirect RF remains highly uncertain in both magnitude and spatial variability (Burrows et al., 2022; Partanen et al., 2014). In contrast, total sea spray aerosol emissions, dominated by (super-micron) sea salt, are much larger ($\approx$ 2000–10 000 Tg yr^{-1}). Despite their far smaller mass, marine organic aerosols are known to exert a disproportionate influence on cloud-forming properties of marine aerosols, driven by amphiphilic biopolymers that suppress droplet surface tension, and facilitate water uptake during activation across successive phytoplankton bloom stages (Kaluarachchi et al., 2022; Kawana et al., 2022; Ovadnevaite et al., 2011b).

Conversely, MSA arises from phytoplankton-derived dimethylsulphoniopropionate (DMSP), cleaved by algal and bacterial enzymes to yield dimethyl sulphide (DMS) which, once ventilated, is oxidised via multi-oxidant pathways (such as OH, NO_3 or halogens) to form MSA and other sulphur species (Goss and Kroll, 2024; Wang et al., 2024). DMS largely dominates the global biogenic sulphur budget and accounts for most of natural sulphur emissions over oceans (Jackson and Gabric, 2022). Globally, DMS burden estimates range from 7.5 Gg S yr^{-1} (Fung et al., 2022) to 40 Gg S yr^{-1} (Cala et al., 2023) and $\sim$ 20.3 Tg C yr^{-1} (Hulswar et al., 2022), with estimated radiative cooling effects ranging from -1.69 to -2.3 W m^{-2} (Fiddes et al., 2018). While MSA contributes only weakly to radiative forcing (Hodshire et al., 2019), it provides a direct tracer of marine biogenic sulphur and DMS oxidation, with implications for both particle formation and growth to cloud condensation nuclei (CCN) relevant sizes (Rosati et al., 2022; Wollesen de Jonge et al., 2021).

Although links between phytoplankton communities and marine aerosols have been demonstrated across multiple studies (Freney et al., 2021; Schwier et al., 2017; Trueblood et al., 2021), the coupling remains uncertain as substantial variations in ocean physics (i.e. mesoscale eddies; Becker et al., 2025) and geochemical variations in epipelagic organics (Lawler et al., 2024; Lowenstein et al., 2025; Seidel et al., 2022) exist across seasons, years and oceanic regions.

At basin scale, these heterogeneities are commonly described using the "Longhurst" biogeochemical provinces, which partition the ocean into regions defined by temperature, turbulence, salinity, nutrient supply, light availability and ecosystem structure (Longhurst, 2007). These ecosystem contrasts imply large variability in the composition of the oceanic organic pool (encompassing a global marine carbon pool of $\sim$ 662 Pg, comparable to the present atmospheric CO_2 burden; Seidel et al., 2022) transferred to the atmosphere via sea spray. Consequently, the impact of these ecosystem contrasts on aerosol production remains potentially significant yet poorly constrained because of complex formation mechanisms and limited ecosystem-level understanding (Seidel et al., 2022; Sellegri et al., 2021). For example, phytoplankton bloom decline is shaped by a suite of biological interactions (Lima-Mendez et al., 2015) that remain completely absent from current PMOA source frameworks.

Consistent with this biological control on marine aerosols production framework, fresh phytoplankton blooms have been reported to account for over two-thirds of global PMOA mass fraction and up to $\sim$ 80 % in the Arctic (Beaupré et al., 2019; Gu et al., 2023). While isotope analysis remains a benchmark for phytoplankton-aerosol coupling, this method provides limited temporal resolution and cannot resolve specific phytoplankton sources. Hence, to advance understanding of phytoplankton-aerosol coupling, there is a need to develop a more integrative framework based on online measurements (Crocker et al., 2020).

Previous studies have revealed direct associations between atmospheric measurements and diatoms (Eickhoff et al., 2023; Ickes et al., 2020; Thornton et al., 2023), haptophytes (Alsante et al., 2025), dinoflagellates (Wieber et al., 2025), *Prochlorococcus* and other prokaryotes (Dall'Osto et al., 2022; Wolf et al., 2019), chlorophytes (Thornton et al., 2023) and cryptophytes (Trueblood et al., 2021); yet, such studies remain scarce and some PFT (e.g. pelagophytes) or other species still remain understudied (Bar-On and Milo, 2019; Moallemi et al., 2021). This work aims at responding to these challenges by using observations from the Mace Head Atmospheric Research Station, a long-term Northeast Atlantic site that frequently samples clean marine air masses influenced by regional phytoplankton activity. Here we thus combine a full year of high-resolution aerosol mass spectrometry measurements with organic aerosols source apportionment and air-mass exposure to eight phytoplankton functional types (PFTs) and micronekton to define origins and properties of PMOA and MSA.

2 Materials and Methods

2.1 Site Description

The Mace Head Atmospheric Research Station is strategically located on the west coast of Ireland at 53°19′ N, 9°54′ W in Connemara, County Galway. Positioned approximately 100 m from the Atlantic Ocean coastline at 5–21 m above sea level, the station provides an exceptional vantage point for atmospheric monitoring (O'Dowd et al., 2014) as the peninsula is exposed to open ocean air masses mostly devoid of anthropogenic influence. These air masses are predominantly steered by westerlies ushered by the polar jet's

low-pressure systems interspersed with episodes of polar or tropical influences (Ovadnevaite et al., 2014b). The station is largely representative of Northern Hemisphere background conditions and is also especially useful for improving our understanding of large scale phenomena such as phytoplankton blooms (O'Dowd et al., 2015) and, more generally, sea spray dynamics over the North-East Atlantic as a whole (Ovadnevaite et al., 2011a; Xu et al., 2022).

2.2 In-situ measurements

Ambient aerosol chemical composition was quantified with an Aerodyne high-resolution time-of-flight aerosol mass spectrometer (HR-ToF-AMS) operating with a 650 °C tungsten vaporizer (DeCarlo et al., 2006). Submicron ambient aerosol was drawn from the community sampling inlet in isokinetic conditions to avoid particle losses (Brockmann, 2011). AMS data processing followed the standard Igor-based procedures (SQUIRREL v1.65B and PIKA v1.25B). Detection limit ($\sim 1\,\mathrm{ng\,m^{-3}}$ for multi-hours organic aerosols blank filters), ionisation efficiency, particle velocity, inlet flow, and composition dependent collection efficiency were determined following standard methods (Drewnick et al., 2009; Middlebrook et al., 2012). Standard relative ionisation efficiency values were applied (Xu et al., 2018). Additionally, MSA was derived by upscaling the $CH_3SO_2^+$ mesylate ion at m/z 78.98 as described in Ovadnevaite et al. (2014b) such as:

$$\mathrm{MSA} = \mathrm{CH_3SO_2} \times 29.12 \times 0.714\ [\mu\mathrm{g\,m^{-3}}] \quad (1)$$

where the numerical coefficients reflect respectively the applied HR-ToF-AMS calibration constants (including nitrate ionisation efficiency) and assumed relative ionisation efficiency for MSA.

Equivalent black carbon (eBC) mass concentrations were also measured with a multi-angle absorption photometer (MAAP, Thermo Fisher Scientific model 5012) operating at a flow rate of $10\,\mathrm{L\,min^{-1}}$ and a 5 min time resolution with optical correction as described in Xu et al. (2020). During the first half of 2018, the MAAP was used to flag pollution events while in the second half of 2018, a dual spot aethalometer (Model 33, Magee Scientific) was used instead with optical correction as described in Fossum et al. (2024). The measurements were used to evaluate anthropogenic influence on the PMF-resolved aerosol factors, without applying any eBC-based data filtering.

2.3 Source apportionment

The IGOR PRO Source Finder (SoFi v9.5.2) toolkit (Canonaco et al., 2013) was used to run the PMF algorithm for the source apportionment. The HR-ToF-AMS error matrix (Corbin et al., 2015) was generated from the PIKA (Peak Integration by Key Analysis) v1.25B software package. Cell-wise downweighing of the organic aerosol matrix was applied such that weak (signal-to-noise ratio, SNR < 2) and poor signals (signal-to-noise ratio, SNR < 0.2, including zero and negative values) were assigned proportionally larger uncertainties to limit their influence on the PMF solution. Primary marine organic aerosol was constrained using reference mass spectra by Ovadnevaite et al. (2011b) with a-values (Canonaco et al., 2013) ranging from 0.1 to 0.9 with steps of 0.1 between 3 to 8 factors and refined a-values of 0.1 to 0.5 with steps of 0.05 for the retained 6 factors final solution (These a-values control how much the model can deviate from the reference spectrum, with lower values enforcing tighter constraints and higher values allowing more flexibility). To evaluate the stability of the PMF solution, a bootstrap resampling approach with a total of 300 runs was applied (Crespi et al., 2016; Efron, 1979). This procedure quantifies statistical uncertainty in the PMF decomposition by evaluating the stability of the resolved PMOA factor across resampled datasets, capturing variability in both its time series and mass spectral profile, as well as the associated rotational ambiguity inherent to the solutions.

2.4 Phytoplankton Functional Types and Micronekton

PFTs were taken from the AI-driven Global Daily gap-free Phytoplankton Functional Type dataset (AIGD-PFT; Zhang et al., 2024a). AIGD-PFT combines in situ HPLC (high-performance liquid chromatography) pigment measurements with OC-CCI v6.0 daily reflectance from SeaWiFS, MODIS, MERIS and VIIRS, together with environmental predictors, within a deep-learning framework that produces gap-free global daily surface fields at 4 km resolution spanning 1998 to 2023. In this work, sea-surface chlorophyll-a concentrations ($\mathrm{mg\,m^{-3}}$) were used for *Prochlorococcus* and other prokaryotes (predominantly picophytoplankton); haptophytes, pelagophytes, cryptophytes and chlorophytes (predominantly nanophytoplankton); and diatoms and dinoflagellates (predominantly microphytoplankton). All PFTs values used in this analysis were well above the approximate detection limit of the underlying HPLC training data ($\sim 0.001\,\mathrm{mg\,m^{-3}}$), and therefore uncertainty associated with low-concentration oligotrophic waters was not considered a limitation here. For comparison, NOAA MSL12 multi-sensor DINEOF global 9 km gap-filled Chl-a and suspended particulate matter (SPM) were retrieved from the COAST-WATCH portal (Liu and Wang, 2022), while particulate organic carbon (POC) was also retrieved from Zhang et al. (2024b) and surface nitrate (NO_3^-), phosphate (PO_4^{3-}) and silicate, $Si(OH)_4$ were extracted from the Copernicus Marine Global Ocean Biogeochemistry Hindcast product (GLOBAL_MULTIYEAR_BGC_001_029) which provides daily PISCES-v2 fields on a regular 0.25° grid (Aumont et al., 2015).

To complement this, epipelagic (i.e. down to 1.5× the local euphotic depth, typically ∼100–200 m) micronekton biomass fields (expressed as $gC\,m^{-2}$ in seawater) were extracted from the Copernicus Marine environment GLOBAL_MULTIYEAR_BGC_001_033 product (European Union-Copernicus Marine Service, 2021). Epipelagic micronekton (e.g., fish, crustaceans and cephalopods) are active swimmers (∼1–20 cm) organised into depth-stratified functional groups with diel migration and explicit behavioural dynamics. Micronekton data are available as 1/12° (∼8 km) daily hindcasts from 1998 onwards, generated with Spatial Ecosystem And POpulation DYnamic Model – Lower and Mid-Trophic Levels (SEAPODYM-LMTL). More specifically, micronekton are simulated as low- and mid-trophic biomass using advection-diffusion-reaction dynamics forced by ocean currents, temperature, and satellite-derived net primary productivity, with a reported mean absolute difference of $\sim 0.44\,g\,C\,m^{-2}$ against observations (Albernhe et al., 2024).

2.5 Air masses and Exposure

The Hybrid Single-Particle Lagrangian Integrated Trajectory (HYSPLIT) model (Stein et al., 2015) was set up with monthly GDAS meteorological data and 72 h-long back trajectories were generated every hour with arrival height set to 100 m above ground level. To investigate potential source regions, the simplified Quantitative Transport Bias Analysis (SQTBA) method was used to robustly represent Gaussian plumes transport bias along air masses (Zhou et al., 2019). Building on SQTBA spatial extent, meteorological and wave parameters were retrieved from the European Centre for Medium-Range Weather Forecasts (C3S, 2018) to investigate source region conditions. Variables included 10 m wind components ($m\,s^{-1}$), sea surface temperature (K), 2 m air and dew-point temperature (K), significant wave height (m), and peak wave period (s). Derived quantities included seawater kinematic viscosity ($m^2\,s^{-1}$) assuming a constant salinity of 35 PSU, atmospheric stability (the air-sea temperature difference), wave age and the Reynolds wave number following Markuszewski et al. (2024) and Ovadnevaite et al. (2014a). Whitecap coverage was estimated from 10 m wind speed (Callaghan et al., 2008) and used to constrain the breaking-wave air-entrainment flux (Deike et al., 2022). Submicron bubble cap and film flapping production during bubble bursting was calculated assuming a fixed seawater capillary length of 2.7 mm (Deike et al., 2022). For context, surface-tension measurements in natural seawater, including biologically active waters imply capillary lengths of approximately 2.4–2.8 mm, assuming a seawater density of $1025\,kg\,m^{-3}$ (Long et al., 2014; Sellegri et al., 2023a). Finally, the bubble penetration depth in the ocean was scaled using significant wave height and the effective wind-couple wavelength (Cifuentes-Lorenzen et al., 2023).

The air masses exposure to surface ocean biology was then adapted from the literature assuming that submicron aerosols are well mixed within the boundary layer with the 72 h window being consistent with the preservation of sea spray chemical makeup (Gamage et al., 2025). Exposure was set to zero at trajectory endpoints with pressures below 850 hPa, affecting 6 % of trajectories and boundary layer heights below 50 m were set to 50 m which accounted for 2.6 % of trajectories (Yan et al., 2024). Values were calculated as the geometric average within a 20 km radius of each trajectory endpoint (Liu et al., 2022) since ocean biological surface activity is known to follow a log-normal distribution (Campbell, 1995). To determine air masses origin, the retention times over land and marine boundary layer were determined to exclude air masses with substantial terrestrial influence or weak coupling to surface marine emissions (Yan et al., 2024). Furthermore, to evaluate the influence of methodological choices on the exposure estimates, sensitivity tests were performed for both the trajectory radii and trajectory lifetime (Figs. S1–S2 in the Supplement). Given that fronts and eddies can move up to 50–80 $km\,d^{-1}$ (Gangrade and Mangolte, 2024), radii of 20–80 km were tested and yielded consistent exposure time series, indicating limited sensitivity to buffer size. Similarly, varying the back-trajectory duration from 24 to 72 h showed broad consistency in the exposure signal with Pearson's correlations always exceeding 0.7.

2.6 Time series and Lags Analysis

Changepoints (i.e. blooms regime shifts) were identified in phytoplankton exposure time series using the *EnvCpt* R package (Killick et al., 2018). Exposure time series contained small filtered gaps (∼5 % missing values) which were imputed using Kalman smoothing with *na_kalman* from the *imputeTS* package (Moritz and Bartz-Beielstein, 2017). Covariance among PFT predictors and micronekton was assessed using variance inflation factors (VIFs). All eight PFTs and micronekton were subsequently entered simultaneously into an elastic-net regression. The mixing parameter α and regularisation parameter λ were selected by bootstrapped blocked cross-validation (Zou and Hastie, 2005).

Prior to lag analysis, stationarity was assessed using the augmented Dickey-Fuller (ADF) and Kwiatkowski-Phillips-Schmidt-Shin (KPSS) tests. Across the time series, ADF tests failed to reject the unit-root null hypothesis, whereas KPSS tests rejected stationarity ($p < 0.05$). Because conventional cross-correlation can produce spurious lag structure under non-stationary conditions (Cheng et al., 2021), lag dependence was examined using cross-entropy (Giannerini and Goracci, 2023) which equals zero under independence and increases with nonlinear dependence. In practice, the joint density was estimated from hourly data with a Gaussian product kernel and the normal-reference bandwidth (Giannerini and Goracci, 2023). Dependence was evaluated for lags of 0 to 30 d, separately for the spring-summer climax

and the August depletion phase. Statistical significance was assessed against surrogate data (Theiler et al., 1992). The aerosol time series was left unchanged, and the PFT were replaced by iterative amplitude-adjusted Fourier transform (IAAFT) surrogates (Schreiber and Schmitz, 1996). Multiplicity was controlled with a resampling-based step-down max-T procedure. Lags with a per-lag $p \leq 0.05$ over at least 6 consecutive hours are marked and the maximum of each such interval is reported, 6 h being the analysis cycle of the GDAS fields driving the back trajectories.

3 Results and Discussion

3.1 Temporal Dynamics and Biogeographic Patterns of Phytoplankton Functional Types

Daily biomass fields for major PFTs are first assessed against known established ecological seasonal and regional patterns to ensure model qualitative consistency with literature. Figure S3 shows the North Atlantic weighted averages time series of seasonal dynamics of PFT biomass over a full year (2018) overlaid with changepoint analysis structural breaks. The weighted average is made from every grid cell retrieval from the region bounded by 20–66° N and 72–0° W longitude (Fig. S4), similar to Mansour et al. (2024).

Changepoint analysis shows a temporally ordered succession consistent with canonical bloom dynamics as diatoms enter the spring-summer climax phase on 16 March, followed by dinoflagellates on 6 April, haptophytes on 17 April, and chlorophytes on 30 April, consistently with typical PFT succession (Needham and Fuhrman, 2016). The diatoms climax phase persists until 17 July, after which their relative biomass declines steadily as diatoms are expected to progress into the stratified nutrients-limited depletion phase (Behrenfeld et al., 2019). Further autumn to winter restructuring is also observed with *Prochlorococcus* and other prokaryotes increasing on 22 September, and subsequent prokaryotic reorganisations on 6 and 20 December as the winter transition to deep mixing conditions sets in Behrenfeld et al. (2019). This increase is also consistent with the well-known rise in prokaryotes following seasonal entrainment of thermocline material and deep-ocean taxa into surface waters (Wenley et al., 2021) whereas their strongly fluctuating standard deviation reflects patchy mesoscale filaments and eddy structures typical of prokaryotes (Gray et al., 2024).

To further explore spatial variability in surface concentrations, AIGD-PFT data are split into bioregions following Longhurst biomes delineation (Longhurst, 2007) (Fig. 1) with respective contributions (%) to PFT chl-*a* biomass shown in Table S1 in the Supplement. Overall, throughout the year and all Longhurst provinces, diatoms biomass is prevailing (19.4 %–65.5 %), only closely followed by chlorophytes (15.7 %–32.3 %), haptophytes (4.7 %–23.7 %) and cryptophytes (5.2 %–8.7 %). Dinoflagellates remain relatively constant across basins (∼ 5 %), consistently with the ∼ 5 % relative abundance reported in previous field studies in the Western North Atlantic (Wang et al., 2021) and in the subtropical North Atlantic (Duhamel et al., 2019). In contrast to this, *Prochlorococcus* (0.9 %–7.6 %) and other prokaryotes (0.6 %–6.7 %) display a clear south-north concentrations gradient, with higher contributions at lower latitudes (consistent with observations of increasing cyanobacterial dominance toward subtropical regions; Bolaños et al., 2021) whereas pelagophytes remain minor (0.9 %–3.1 %). In addition, haptophytes visibly decline in the boreal polar region (4.7 %), where diatoms are known to outcompete them (Krisch et al., 2020; Pierella Karlusich et al., 2025). Overall, the relative ordering of total surface phytoplankton biomass across Longhurst provinces is consistent with in-situ Atlantic transect observations, with lowest biomass in oligotrophic gyres and enhanced biomass in subpolar and shelf regions (Brotas et al., 2022).

3.2 Primary marine organic aerosol

To robustly estimate PMOA time series, PMOA was constrained using its characteristic mass spectral fingerprint previously established at Mace Head (Ovadnevaite et al., 2011a) and shown in Fig. S5. PMOA mass spectra comprise oxygenated carbons (CHO-type fragments) that dominate the mass spectra intensity (55 %), followed by aliphatic fragments (C_xH_y) contributing 39 %. Representative ion series include C_xH_{2y-3}(i.e. m/z 39.02, 53.03, 67.05, 81) for alkynes, dienes and cycloalkenes, $C_xH_{2y-1}CO$ (i.e. m/z 55.02, 69.03, 83.05) related to alkenyl groups, diunsaturates, cyclic alcohols, and ethers as well as C_xH_{2y+1} (i.e. m/z 15.02, 29.03, 37.00) reflecting alkyls fragments. Further descriptions and implications of PMOA fingerprint are provided in earlier Mace Head studies (Chevassus et al., 2025; Ovadnevaite et al., 2011a). For low factor solutions (3–5 factors; Fig. S5), the retrieved PMOA time series across all a-values show unrealistic behaviour, with large spikes and artificial co-variability with eBC ($R = 0.35$–0.62, Fig. S6). Also, the six-factor solution provides a physically consistent representation, minimising correlation with eBC ($R = 0.16$, Fig. S7). Seven or eight-factor solutions were not retained, as they showed the same PMOA correlations with external tracers as six factors, and furthermore, recent work also indicates that Mace Head submicron aerosols are best represented by six factors (Moschos et al., 2026). Bootstrap diagnostics further support the selection of the six-factor solution (Fig. S8). The reconstructed PMOA time series is stable across resamples, with uncertainty remaining small relative to peak amplitudes (Fig. S8A). The Q/Q_{exp} ratio decreases from 1.24 ± 0.02 (3 factors) to 1.03 ± 0.02 (4 factors), 0.88 ± 0.02 (5 factors), and 0.71 ± 0.02 for the six-factor solution (Fig. S8B). The relative Q/Q_{exp} variability stabilises beyond five factors (Fig. S8C), and the incremental improvement in Q/Q_{exp} becomes marginal after seven factors (Fig. S8D). Residuals for the six-factor solution remain

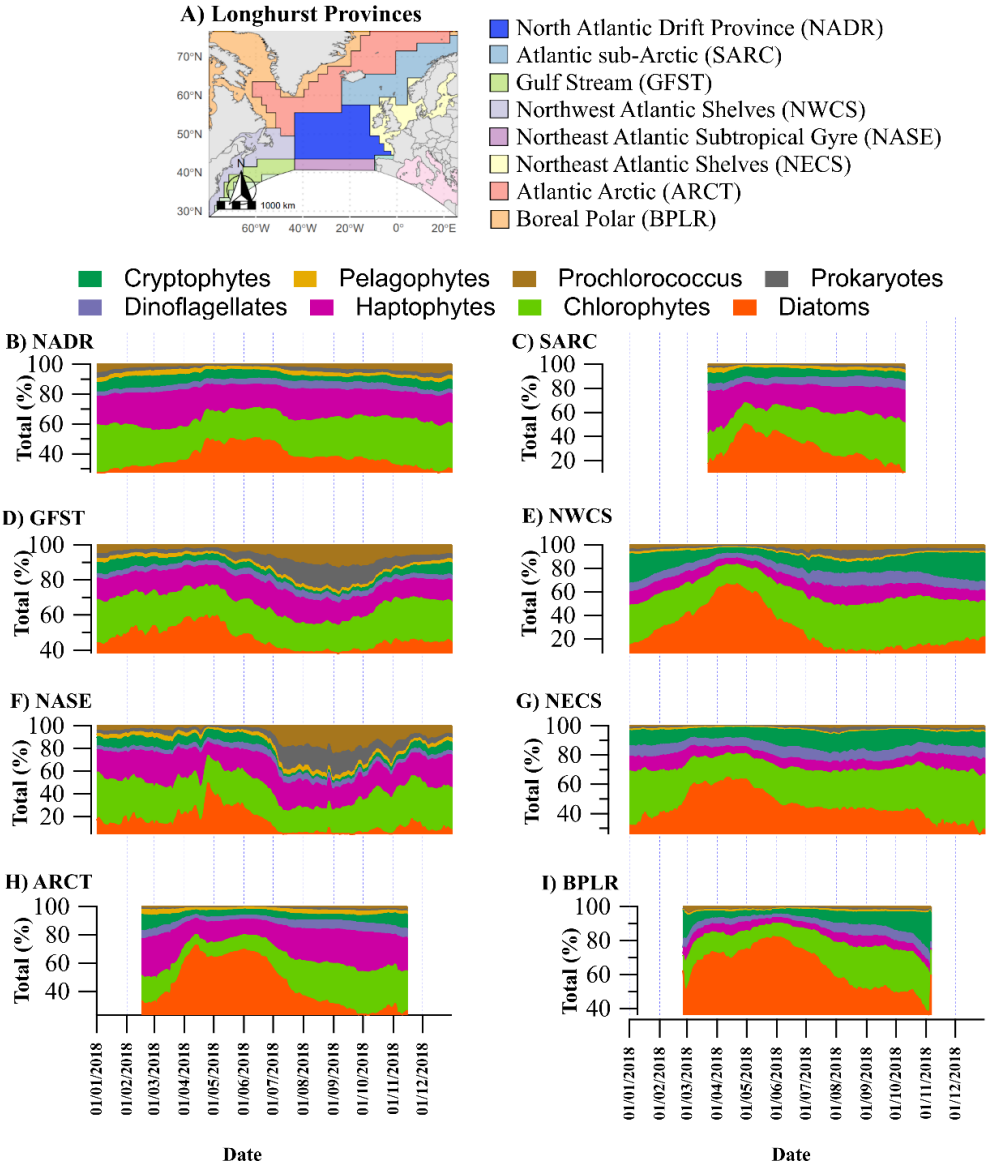


Figure 1. Weighted averages of Phytoplankton functional types by Longhurst regions. BPLR: Boreal Polar, NADR: North Atlantic Drift, GFST: Gulf Stream, ARCT: Atlantic Arctic, SARC: Atlantic Subarctic, NASW: Northwest Atlantic subtropical gyre, NASE: Northeast Atlantic subtropical gyre, NECS: Northeast Atlantic shelf, NWCS: Northwest Atlantic shelf.

randomly distributed without systematic structure (Fig. S8E) and finally, the bootstrap-derived uncertainty distribution is moderately skewed but well constrained (Fig. S8F).

The PMOA times series from the six-factor solution is presented in Fig. 2 as a dashed blue line. PMOA concentrations peaked in late spring-early summer, with a sharp maximum in early July, reflecting the PFT bloom climax. Concentrations then declined through late summer (August), when contemporaneous PMOA-PFT correlations were also low (Fig. S9) and remained low during autumn-winter with only minor fluctuations (Fig. S10). Three contrasting cases were then selected: The Northeast Atlantic shelf (NECS) during phytoplankton bloom climax (25 May to 13 July 2018) and the North Atlantic drift province (NADR) during late summer early depletion (Both August 2018 and August 2009, with the latter featuring PMOA concentrations one order of magnitude higher than August 2018).

3.3 Exposure to phytoplankton functional types, micronekton and collinearity

Since AIGD-PFT can capture real world phytoplankton growth dynamics, with coherent ecological succession across space and time, the associations of these dynamics with marine aerosols are examined next. During the spring-summer climax bloom, PMOA closely covaries with recent biological

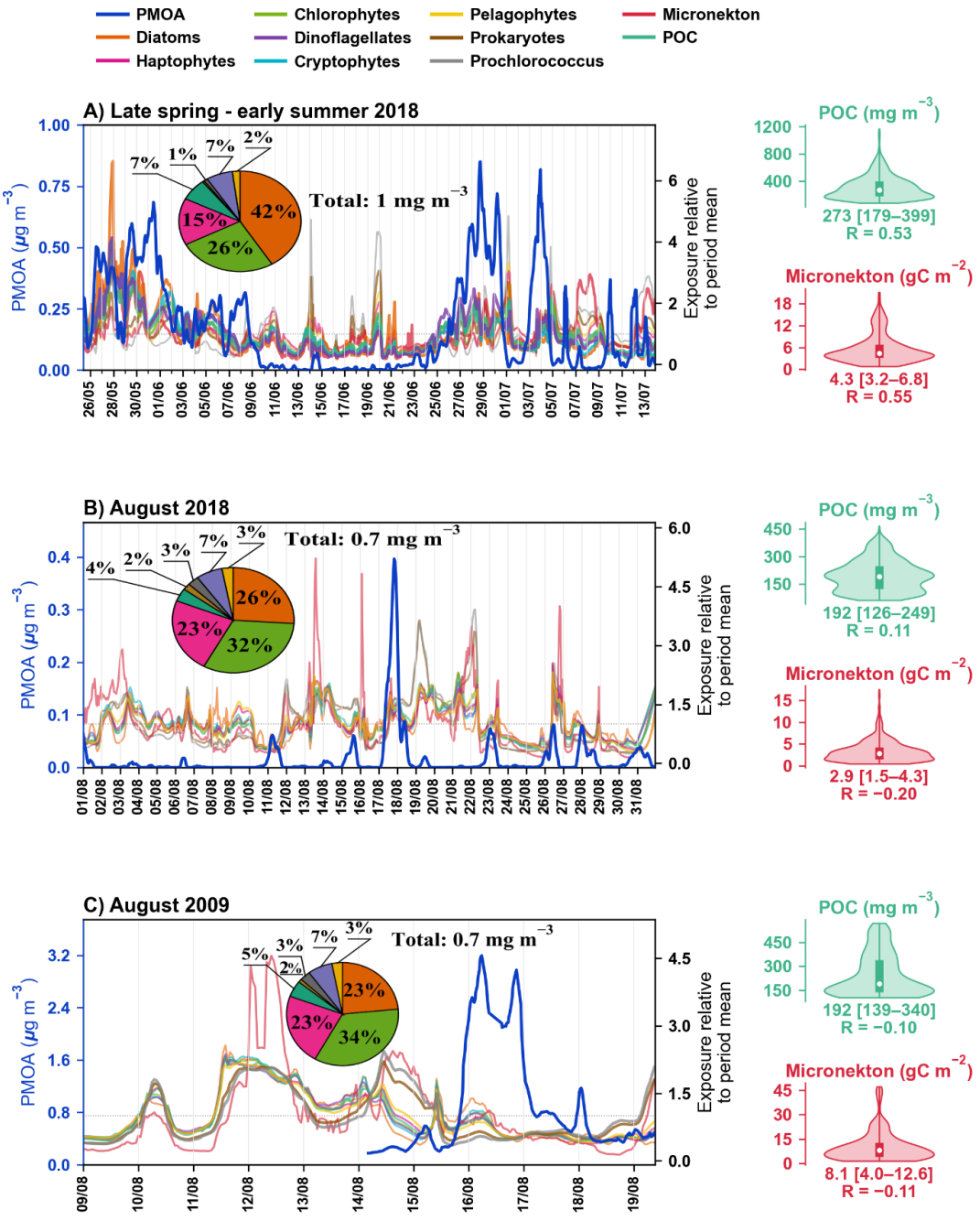


Figure 2. Primary marine organic aerosol (PMOA) time series and associated phytoplankton functional type (PFT) air masses exposure for **(A)** Climax phase – 25 May to 13 July 2018, **(B)** Depletion phase – August 2018, and **(C)** August 2009. PMOA concentrations (left *y*-axis; dashed blue lines) are shown together with the cumulative PFT exposure along the 72 h back trajectories (right *y*-axis). Insets report the relative PFT composition (percentage contribution and total exposure) for each period. Violin plots on the right show the distributions of POC and micronekton exposure with the median [Q1–Q3] and Pearson correlations with PMOA.

activity (Fig. 2A), with strong correlations for dinoflagellates ($R = 0.70$), cryptophytes ($R = 0.68$), diatoms ($R = 0.65$), and chlorophytes ($R = 0.62$). Conversely, haptophytes ($R = 0.30$), prokaryotes ($R = 0.32$), and pelagophytes ($R = 0.21$) exhibit weaker connections, while *Prochlorococcus* shows no measurable relationship ($R = -0.02$).

Furthermore, these PFT correlation coefficients are partly in line with values presented in literature (Table S2) although correlation coefficients are expected to be specific to sampling location and are generally lacking for the North Atlantic. For instance, the HR-ToF-AMS correlations with the main PFT obtained here ($R = 0.62$–0.70) are comparable to

those reported for sea spray fluorescence (SSF) and chlorophytes in the Southern Ocean (Moallemi et al., 2021), similar to those found for haptophytes in the Mediterranean (Sellegri et al., 2021) but lower than the strong correlations with diatoms observed in the Amundsen Sea (Jung et al., 2020). Conversely, diatoms and dinoflagellates relationships fall within the same range as CCN-based correlations (Schwier et al., 2017) reported for the Mediterranean ($R \approx 0.60$), except for *Prochlorococcus* (Schwier et al., 2015) which shows negligible association here while the link with cryptophytes is substantially stronger in this study than the weak or absent relationships found between PMOA and cryptophytes in the Mediterranean (Freney et al., 2021; Trueblood et al., 2021). In contrast to this spring-summer climax, the early depletion phase North Atlantic open-ocean (NADR) PMOA source in August 2018 (Fig. 2B) or August 2009 (Fig. 2C) are characterised by PFT spikes preceding PMOA variability which weakens the apparent contemporaneous correlations (Fig. S10) and instead suggests a more lagged response, investigated in Sect. 3.5.

To assess whether the strongest PMOA-PFT correlations remained distinguishable after accounting for shared bloom variability, elastic net regression was applied jointly to PFT and micronekton exposure during the spring-summer climax. The analysis yielded a global correlation of $R = 0.62$ and highlighted substantial covariance among the PFT predictors (Sect. S1). The ridge solution reproduced the upper tier identified from the individual correlations, with the largest positive standardised coefficients for dinoflagellates ($\beta = 0.18$), cryptophytes (0.15), diatoms (0.12), micronekton (0.12) and chlorophytes (0.10). Haptophytes (0.010) and other prokaryotes (0.042) had smaller positive coefficients, while *Prochlorococcus* (-0.089) and pelagophytes (-0.055) had negative conditional associations.

Furthermore, air-mass exposure to micronekton (Fig. 2) had median [interquartile range] values of 4.3 [3.2–6.8] $\mathrm{gC\,m^{-2}}$ in spring–summer 2018, 2.9 [1.5–4.3] $\mathrm{gC\,m^{-2}}$ in August 2018, and 8.1 [4.0–12.6] $\mathrm{gC\,m^{-2}}$ in August 2009 with PMOA-micronekton correlations ($R \approx 0.55$, -0.20, and -0.11, respectively) following the same structure as PFT, with micronekton spikes also preceding PMOA (Fig. S10). PMOA-micronekton variations align in a first-order sense with previous Arctic measurements reporting substantial enrichment of humic-like organic material in PMOA (40 %–280 % relative to seawater) associated with delayed zooplankton grazing and excretion processes (Dall'Osto et al., 2025). Micronekton concentrations were nearly 3 times higher in August 2009 than in August 2018 coinciding with an almost one order of magnitude elevation in PMOA concentrations, although this also reflected more efficient air-sea transfer conditions as detailed below.

3.4 Source regions, air-sea physics and nutrients

To further investigate biology and air-sea interactions interplay, PMOA Source regions are identified using simplified quantitative transport bias analysis and two dominant source regions were resolved below: The North Atlantic Drift (NADR) region and the Northeast Atlantic shelf (NECS) region (Fig. 3).

To evaluate whether source-region conditions could modulate PMOA through biological processing, macronutrients and POC were compared across the spring-summer 2018 NECS climax and the two August NADR footprints (Table S5, Fig. S12). The spring-summer climax held 1.53-fold more POC than the August 2018 depletion phase, whereas the August 2018 nutrient footprint contained 20.6-fold more nitrate and 4.9-fold more phosphate but 25.7 % less silicate (Table S5). The climax phase combined high host biomass with strong nitrate and phosphate drawdown, conditions that are known to limit viral propagation through reduced host physiology and reduced burst size despite abundant potential hosts (Flynn et al., 2021; Maat and Brussaard, 2016). Along with this, silicate limitation has been shown to facilitate viral infection and accelerate virus-induced mortality in diatoms (Kranzler et al., 2019).

The spring-summer climax, therefore, combined greater PFT and micronekton biomass and a larger POC reservoir with nutrient conditions limiting viral lysis, whereas the August 2018 footprint contained fewer potential hosts but nutrient-replete conditions favouring viral lysis within the remaining phytoplankton community. High PFT biomass and POC could therefore support rapid PMOA production during the climax phase, with viral processing potentially sustaining additional organic-matter release during bloom decline (Mojica and Brussaard, 2026).

These contrasts were superimposed on SST differences that can modify both biological conditions and the bubble-mediated transfer of seawater organic matter to the atmosphere. Median SST was 13.4 °C during the NECS climax, 15.1 °C in August 2018 and 12.5 °C in August 2009 (Table S5, Fig. S13), all above the < 8 °C regime in which Sellegri et al. (2023a) observed an approximately four-fold enhancement of sea-spray flux. The corresponding seawater kinematic viscosity was 4 % higher during the climax and 7 % higher in August 2009 than in August 2018 (Table S5, Fig. S14). Although viscosity differed little, the net influence of SST on PMOA remains unresolved because temperature affects multiple physical and biological processes with competing effects:

Cooler waters can enhance PMOA production in several ways. Microbial degradation of organic matter is slower at lower temperatures (Guadayol et al., 2021; Marsay et al., 2015) which is consistent with POC concentrations being approximately 1.5-fold higher in the two cooler footprints (the spring-summer climax and August 2009) than in the warmer August 2018 footprint (Table S5). Higher viscos-

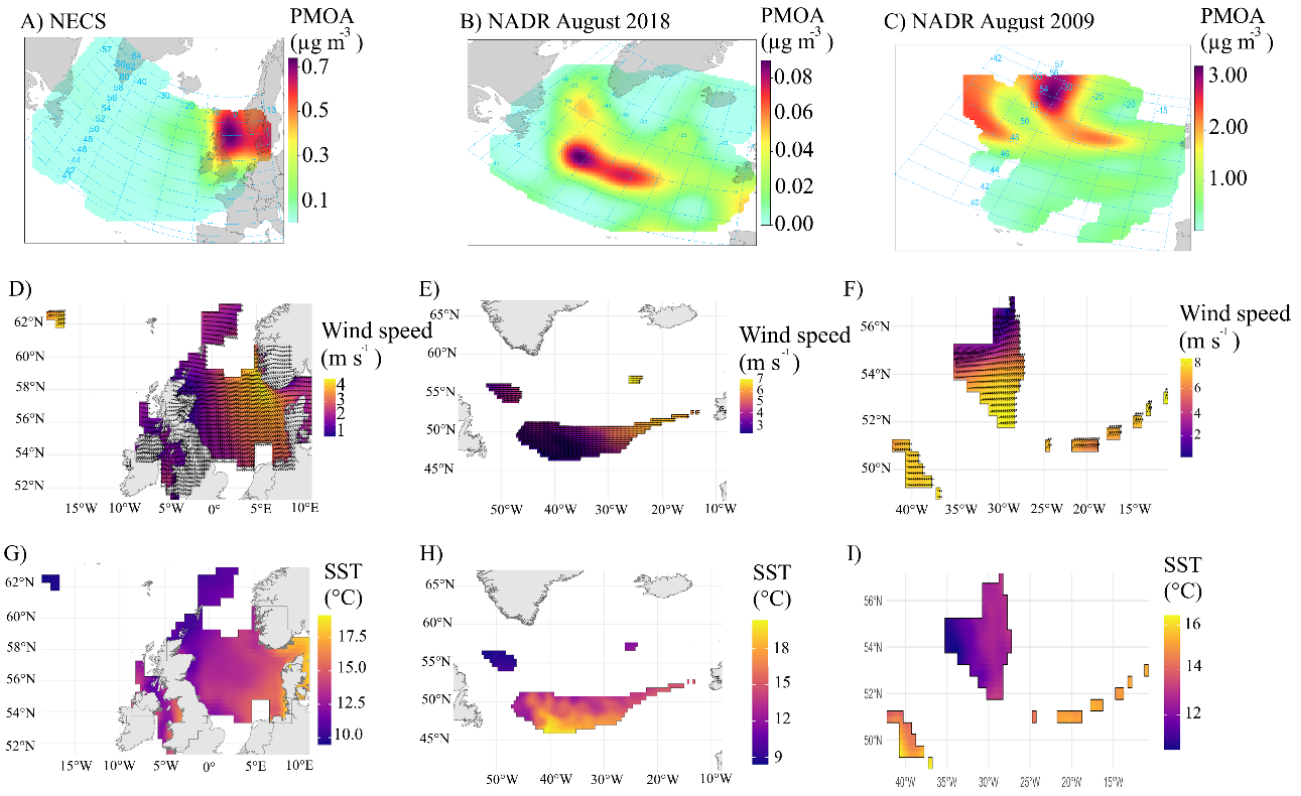


Figure 3. Simplified quantitative transport bias analysis (SQTBA) for primary marine organic aerosol during **(A)** 25 May to 13 July 2018, **(B)** August 2018, and **(C)** August 2009. Panels **(D)**–**(F)** show the corresponding 10 m wind speed fields from ERA5 for the same periods, and panels **(G)**–**(I)** show the associated sea-surface temperatures (SST). Each map displays only the grid cells contributing to the top 10 % of the PMOA back-trajectory mass concentrations footprint for each event.

ity can also reduce the rise velocity of small bubbles, increasing their residence time in the water column but also their susceptibility to dissolution before reaching the surface. Greater POC preservation could increase the persistence of surface-active material available for bubble scavenging through Langmuir-type adsorption onto bubble interfaces which is itself slightly favoured in cooler waters (Burrows et al., 2022). Cooler and more viscous bubble films, together with surfactant-stabilised interfaces, may also further delay film drainage and coalescence and favour transfer at the sea-air interface (Hu et al., 2024; Ribeiro and Mewes, 2006). In addition, colder SST may also increase the degree of lipid unsaturation in planktonic membranes as part of a homeoviscous adaptation that preserves membrane fluidity and enzymatic activity (Holm et al., 2022; Liu et al., 2025a) likely also contributing to the increased POC over the colder SSTs.

However, other temperature-dependent processes act in the opposite direction. Warmer temperatures enhance molecular diffusion and the collision-mediated incorporation of adsorbed material into submicron film drops (Liu et al., 2026), and also alter bubble bursting behaviour and the aerosol yield per bubble (Leibensperger Iii et al., 2026). Moreover, surfactants are known to either enhance or suppress particle production, with a temperature dependence of their own (Modini et al., 2013; Sellegri et al., 2023b), whereas small bubbles rise more slowly in more viscous water and are therefore more likely to dissolve before reaching the surface, which would partly offset the enhanced preservation and scavenging of surface-active material (Callaghan et al., 2014).

The larger separation among the three periods further emerged when this temperature dependence was considered together with the wind and wave forcing that controls bubbles generation, white caps and film drop production. Air-sea conditions became progressively more unstable and the parameterised whitecap coverage increased from the climax to August 2018 and was highest in August 2009 (Table S5, Fig. S14), consistent with increasingly favourable conditions for sustained wave breaking (Callaghan et al., 2008; Markuszewski et al., 2024). Similarly, the median 10 m wind speed increased from 5.45 m s^{-1} (interquartile range: 3.82–6.45 m s^{-1}) during the climax to 6.76 m s^{-1} (6.29–7.55 m s^{-1}) in August 2018 and 9.10 m s^{-1} (7.94–9.88 m s^{-1}) in August 2009 (Table S5). The stronger winds in August 2009 sustained wave breaking (Figs. S14–S15), which is known to increase the probability of bubbles resurfacing and bursting (Czerski et al., 2022). In addition, wind speeds above 4–6 m s^{-1} are known to disrupt the bacterioneuston (Rahlff et al., 2017), mixing surface organic mat-

ter and bacteria into the upper water column, where they become more readily accessible to rising bubbles. Between the spring-summer and August 2018 phases, significant wave height, whitecap coverage and entrained-air flux increased by 45 %, 54 % and 45 %, respectively, whereas the wave Reynolds number and the parameterised film-drop number flux increased by only 6 % and 14 %, and the bubble-plume penetration depth remained at 0.7–0.8 m (Table S5, Fig. S15). Physical forcing was therefore comparable or stronger in August 2018, and yet the strong PFT-PMOA covariance observed during the climax was delayed (Sect. 3.5) which is thus unlikely to be explained by a collapse in the physical capacity to produce sea spray.

Air-sea transfer conditions in August 2009 stood out in particular. Compared to the climax, the wave Reynolds number was 3.2 times higher, whitecap coverage 4.5 times, air entrainment 5.2 times and the parameterised film-drop production 4.0 times higher, which are the highest values of the three periods (Table S5) and are consistent with intense wave breaking and bubble bursting (Deike et al., 2022; Jiang et al., 2022). Furthermore, the wave-age-constrained penetration diagnostic indicated a considerably deeper bubble plume of about 2.0 m (Table S5), compared to 0.7–0.8 m in both 2018 periods (Cifuentes-Lorenzen et al., 2023).

Overall, the three periods identify distinct combinations of biological source strength and physical transfer. The spring–summer 2018 climax combined a large, actively produced POC reservoir, strong nitrate and phosphate drawdown combined with bubble-mediated transfer that appeared sufficient to preserve the covariance between PFT, micronekton, and PMOA. In August 2018, physical forcing was stronger, but the POC reservoir was about one third smaller (Table S5). This suggests that increased mechanical forcing alone without the proper biological conditions is insufficient to sustain PMOA variability.

Conversely August 2009 combined a sufficient POC reservoir with the strongest wave breaking, air entrainment, bubble-plume development and film-drop production and highest micronekton exposure, providing favourable conditions for efficient POC aerosolisation although the PFT-PMOA variability shifted toward a more lagged response. This may reflect both stronger physical integration of a pre-existing organic reservoir and influences of SST and nutrients on viral lysis and grazing.

Taken together, the contrasting conditions help clarify why PMOA amplitudes differ across periods with similar phytoplankton exposure and hint at PMOA plumes spiking after PFT increase with more or less delay, as such, temporally resolved approaches are next explored to disentangle genuine source-receptor dynamics.

3.5 Lag estimates

Biological production and subsequent organic-matter processing operate on different timescales, which motivates the following analysis of lagged relationships between biological exposure, PMOA, and MSA. Chl-*a* is the proxy most commonly used to link ocean biology to marine organic aerosol, and both chl-*a* and SPM were therefore tested first. Neither performed well. Their raw time series correlated only weakly with PMOA ($R = 0.43$ and 0.28), reaching values comparable to the PFTs only after Hampel outlier filtering ($R = 0.59$ and 0.60), and their cross-entropy with PMOA was weakly significant at 2–4 d only (Fig. S16). For chl-*a* this is not surprising, since it is not a stable measure of biomass. Nutrient stress changes the chlorophyll content of cells independently of their biomass and growth rate (Kruskopf and Flynn, 2006), which matters here given the strong nitrate and phosphate drawdown of the climax (Sect. 3.4), and chl-*a* also responds to light-driven physiological adjustments (Liu et al., 2025b) and to optical interference from lysis by-products and post-bloom organic matter (Prochaska and Frouin, 2024; Simis et al., 2007). Its reliability as a productivity proxy consequently degrades over senescent blooms and oligotrophic waters (Collins et al., 2016), which limits the generality of the relationship reported between lag-adjusted chl-*a* and sea spray organics (O'Dowd et al., 2015). The lag analysis below therefore relies on PFT and micronekton exposure, which requires no outlier filtering and draws on pigment data in which degradation products are treated explicitly (Zhang et al., 2024a).

The climax period corresponds to a single prolonged phytoplankton bloom identified by the changepoint analysis from 25 May to 13 July (Sect. 3.1). For PMOA during the spring-summer climax phase, PMOA-PFT cross entropy is highest at zero lag for diatoms (per-lag $p = 0.007$), dinoflagellates ($p = 0.006$) and cryptophytes ($p = 0.023$), with a second interval at about 2 d for the same three taxa ($p =$ 0.023 to 0.042), whereas chlorophytes show no lags (Fig. 4a). Later maxima are found for haptophytes at 21 d ($p = 0.016$), pelagophytes at 22 d ($p = 0.013$), other prokaryotes at 13 and 21 d ($p = 0.004$ and 0.009) and *Prochlorococcus* at 13 d ($p = 0.003$). Overall, cross-entropy scores from haptophytes, *Prochlorococcus* and pelagophytes (peak S_ρ of about 0.03) were about half those of dinoflagellates, cryptophytes and diatoms (0.06–0.07), with chlorophytes and other prokaryotes in between (0.045). This might be explained by *Prochlorococcus* being a comparatively less intense lipid emitter (Becker et al., 2025) whereas pelagophyte biomass is extremely small over the North Atlantic (2.7 %). Distinct lag patterns among PFTs are also compatible with diatoms, haptophytes and cyanobacteria each producing different metabolite suites (Heal et al., 2021). Given the strong collinearity among PFTs (Sect. 3.3), these lags are best read as distinguishing two groups of intercorrelated taxa, the bloom-forming group and a second group formed by haptophytes, pelagophytes and the prokaryotes.

Diatoms, dinoflagellates and cryptophytes all have similar PMOA lags, with a concurrent and early-bloom-stage response (0–2 d), whereas the later maxima (13–21 d) ap-

pear in haptophytes, pelagophytes and prokaryotes taxa for which viral lysis is known to release different organic compounds in comparison to early exudates (Kuhlisch et al., 2021; Ma et al., 2018). The concurrent and early response (0–2 d) of diatoms, dinoflagellates and cryptophytes fits the conditions of the NECS climax described in Sect. 3.4: high host biomass under strong nitrate and phosphate drawdown, where nutrient-limited cells release carbon-rich exudates (Thornton, 2014) while viral propagation is restrained (Maat and Brussaard, 2016), so that PMOA tracks the living bloom. This concurrent dependence is what the contemporaneous correlations of Sect. 3.3 capture. Three of the four taxa with the strongest correlations (dinoflagellates, cryptophytes and diatoms) are those with a zero-lag maximum, whereas haptophytes, pelagophytes and the prokaryotes, which correlate weakly with PMOA at zero lag carry the later maxima.

The later maxima (13–21 d) of haptophytes, pelagophytes and the two prokaryote groups are then consistent with delayed lysis, since nutrients limitation reduces the number of viruses released per lysed cell (Maat and Brussaard, 2016) as discussed in Sect. 3.4. Lysates are also known to differ in composition from early exudates (Kuhlisch et al., 2021; Ma et al., 2018) and continue to be transformed by heterotrophic bacteria over days to weeks (Zhao et al., 2019), which further spreads the response in time while organic matter might also be released before cell lysis and sustained by infection propagation and late-stage prokaryote-diatom interactions (Mojica and Brussaard, 2026; Zamanillo et al., 2019).

Furthermore, micronekton ranks alongside the upper-tier PFTs with maxima at 0 d (per-lag $p = 0.012$) and near 14 d ($p = 0.015$), suggesting that trophic-level processes may contribute to PMOA at magnitudes comparable to direct phytoplankton emissions, plausibly through bubble-mediated enrichment of lipid-rich faecal pellets and excretion products. This is in line with the 1.5-fold higher micronekton concentrations of the climax footprint (Sect. 3.4).

During the August 2018 depletion phase the PMOA lag structure differs markedly (Fig. 4b). The concurrent dependence found during the climax is absent, at zero lag and the peak cross-entropy scores (0.017–0.025) are about one third of those of the bloom-forming taxa during the climax (0.06–0.07). Instead, diatoms, dinoflagellates, cryptophytes, chlorophytes, haptophytes and pelagophytes share a single maximum lag at 27 d, with secondary maxima near 9 d for dinoflagellates, haptophytes and pelagophytes ($p = 0.015$ to 0.034). Other prokaryotes and *Prochlorococcus*, which carried the 13–21 d maxima during the climax, show no interval of at least 6 h with $p \leq 0.05$, only a 5 h exceedance at 9.0 d ($p = 0.035$ and 0.037), and micronekton shows a single maximum at 18 d ($p = 0.015$). A lag of 27 d places the driver signal between 5 July and 4 August, that is at the end of the climax phase. These changing lags during depletion are consistent with a shift from production-driven to lysis-driven release. The August NADR footprint was warmer and nutrient replete (Table S5) with a smaller POC reservoir, and with lower silicate, which is known to facilitate diatoms viral infection (Sect. 3.4; Kranzler et al., 2019). Under these conditions, PMOA carries the legacy of the bloom decline as it undergoes viral lysis (Kuhlisch et al., 2021). The shorter maxima near 9 d are in turn consistent with the faster infection cycles expected in warmer, nutrient-replete water (Maat et al., 2017).

For MSA, cross entropy during the same climax phase shows its largest values for lags of about 4 d for diatoms, dinoflagellates, cryptophytes and chlorophytes, with a secondary maximum near 12 d for diatoms ($p = 0.033$) (Fig. S17a). Haptophytes and pelagophytes show maxima between 21 and 27 d, and other prokaryotes and *Prochlorococcus* between 15 and 27 d. These long lags may reflect *Prochlorococcus* having limited DMSP-cleaving enzyme activity, shifting late-stage DMS production to bacteria, viruses, or enzymes species decoupled from the initial bloom phase (Malfatti et al., 2019). The shared 4 d lags of the bloom-forming taxa are also consistent with the climax phase nutrient drawdown (Sect. 3.4), since low DMSP producers such as diatoms can raise their intracellular DMSP by up to about 16-fold under nutrient stress (McParland and Levine, 2019).

Micronekton cross-entropy with MSA further shows lags at about 4 and 13 d, which is consistent with grazing-driven DMS release followed by atmospheric oxidation, though it does not exclude behavioural aggregation of higher trophic levels along DMS gradients acting as chemosensory cues (Owen et al., 2021) or substantial DMS release from planktivory micronekton or lower-trophic level grazing (e.g. copepods grazing on dinoflagellates; Dacey and Wakeham, 1986). Overall, the PFT-micronekton contributions ranking for MSA is markedly diffuse as MSA is the product of a multi-step pathway (DMSP → DMS → multi-oxidant atmospheric chemistry) where atmospheric oxidation results in homogenised source-specific signatures.

Finally, during the August depletion phase the contrast for MSA runs the other way (Fig. S17b). the single 4 d maximum of the climax is replaced by recurring maxima near 8–9, 14 and 27–30 d for most PFTs ($p = 0.002$ to 0.04), with micronekton at 22.5 d ($p = 0.003$).

Together, these contrasts indicate that the timing of PMOA and MSA associations changes with bloom phase: rapid marine organic aerosols during the climax give way to delayed associations during depletion.

4 Conclusions

By combining a full year of high-resolution aerosol mass spectrometry at Mace Head with HYSPLIT-derived air-mass exposure to gap-free phytoplankton functional type (PFT) and micronekton fields, this study resolves links between marine organic aerosols and ecosystem composition that bulk

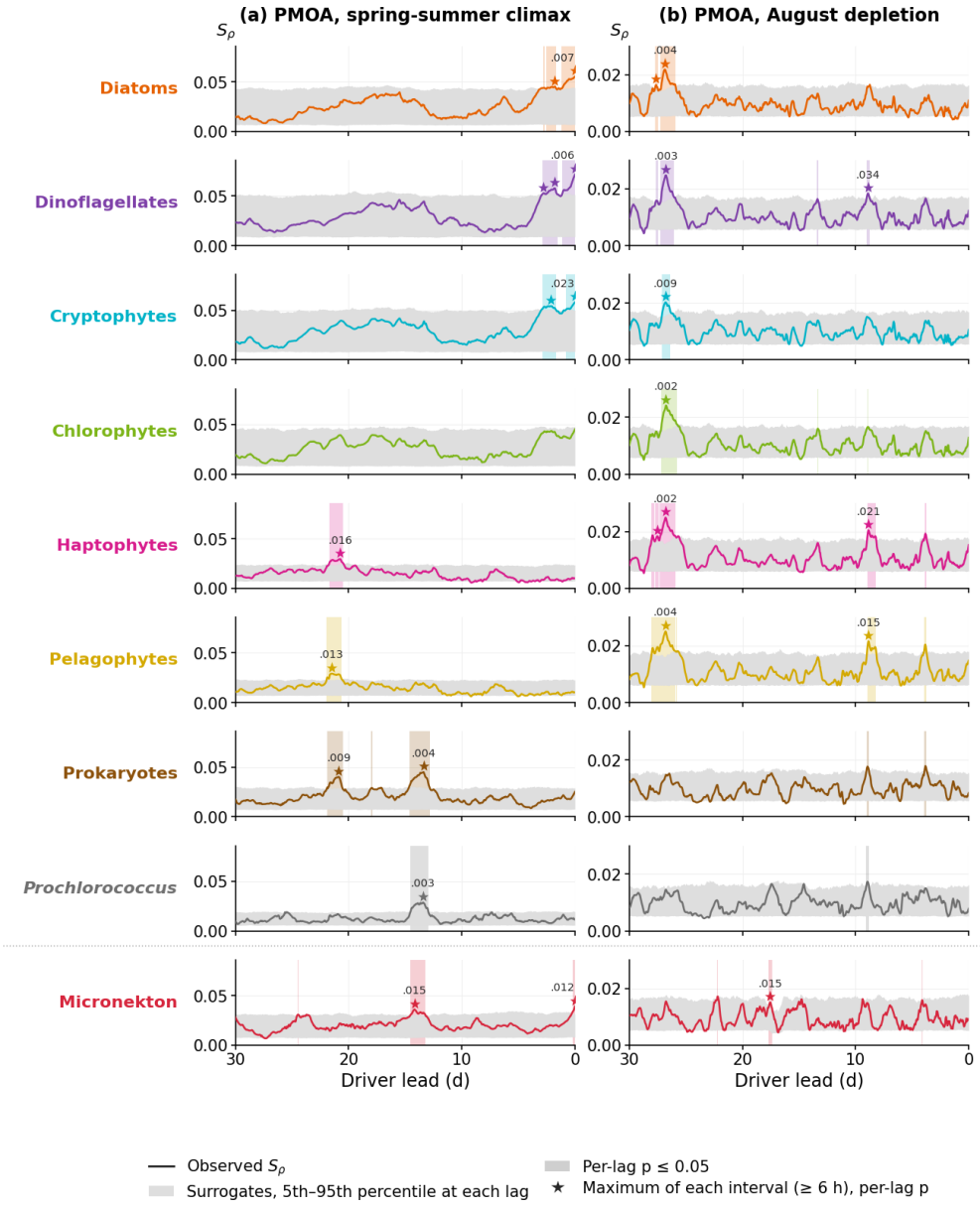


Figure 4. Lagged cross-entropy S_ρ between PMOA and air-mass exposure to the eight phytoplankton functional types (PFTs) and micronekton at Mace Head during **(a)** the spring-summer climax phase and **(b)** the August 2018 depletion phase. Coloured lines show the observed S_ρ, and grey bands show the 5th–95th percentile of 1000 surrogates at each lag (multivariate IAAFT for the PFTs, univariate IAAFT for micronekton). Shading marks lags with a per-lag p value of 0.05 or less, where p is the share of surrogates with S_ρ at least as large as observed at that lag. Stars mark the maximum of each such interval lasting at least 6 h, and the number above a star is the per-lag p value at that maximum. The corresponding MSA lags are given in Fig. S17.

chl-*a* cannot capture. Building on this framework, four key findings emerge and are summarised below.

First, the timing of PMOA-PFT dependence changes with bloom phase. During the spring-summer climax, PMOA showed a concurrent (0–2 d) dependence on diatoms, dinoflagellates and cryptophytes, and later maxima (13–21 d) for haptophytes, pelagophytes and the two prokaryote groups. Given the strong covariance among PFTs, these lags distinguish two groups of intercorrelated taxa, and individual sources could not be isolated. The concurrent response is consistent with nutrient-limited exudation from diatoms dominated blooms (Hansell et al., 2024; Lu et al., 2025), alongside lipid-rich cryptophytes and fatty-acid-producing dinoflagellates (Bi et al., 2019; Taipale et al., 2020), while chlorophytes are major contributors to carbon cycling (Duhamel et al., 2019). Conversely, haptophytes

showed a weaker and delayed dependence, even though they also release aliphatic and alcohol compounds during viral lysis or open-ocean nutrient starvation (Fulton et al., 2014; Malitsky et al., 2016; Rosenwasser et al., 2014), suggesting that lysis-related release lags behind the living bloom. In the August 2018 depletion phase, the concurrent dependence disappeared and most PFTs shared a single maximum at 27 d, pointing back to the end of the climax, consistent with a shift from production- to lysis-driven release. These taxonomic links may however remain context-dependent, as plankton lipidomes vary across regions and assemblages (Liu et al., 2025a).

Second, MSA showed a broader and less taxon-specific signature than PMOA, consistent with the multi-step DMSP-DMS-MSA pathway homogenising source signals. During the climax, diatoms, dinoflagellates, cryptophytes and chlorophytes shared the earliest maximum ($\sim$ 4 d), whereas haptophytes, pelagophytes and the prokaryotes peaked at 15–27 d; in August, these were replaced by recurring maxima near 8–9, 14 and 27–30 d. Although diatoms are low per-cell DMSP producers, their biomass can dominate system-level DMSP production in subarctic blooms (Dani and Loreto, 2017; Jang et al., 2019), and the early response of diatoms along with cryptophytes and chlorophytes supports recent evidence that groups once thought to lack DMSP lyases may be emerging players in the marine sulphur cycle (Bullock et al., 2017; Shemi et al., 2023; Wang et al., 2024).

Third, micronekton exposure ranked alongside the upper-tier PFTs for PMOA, with maxima at 0 and $\sim$ 14 d during the climax and no zero-lag dependence in August 2018 and high concentrations before the August 2009 PMOA maximum. This is consistent with organic-carbon processing through egestion, excretion and mortality (Hernández-León, 2023; Thibault et al., 2025) and with grazing-related enrichment of humic-like material in PMOA (Dall'Osto et al., 2025).

Fourth, phytoplankton-aerosol coupling appeared to be modulated by the combined ecosystem state and air-sea transfer. The spring-summer 2018 shelf climax combined a large POC reservoir and strong nutrient drawdown with sufficient bubble-mediated transfer, whereas August 2018 had lower POC and stronger wave breaking, whitecap coverage and air entrainment. August 2009 combined a higher POC reservoir with the strongest wave breaking, air entrainment, bubble-plume development and film-drop production, coincident with much higher but more lagged PMOA. These contrasts suggest that increased mechanical forcing alone is insufficient to sustain PMOA variability, which reflects the joint influence of biological source strength and physical transfer.

Unresolved processes may further modulate this coupling: surfactant control of bubble film thickness and lifetime (Ovadnevaite et al., 2017; Sellegri et al., 2021), seasonal and regional differences in microbial recycling and viral lysis (Eigemann et al., 2024; Mojica et al., 2016), biological components not represented here, including viruses, archaea and fungal processes such as the fungal shunt (Klawonn et al., 2021), microbial DMS consumption (Le Gland et al., 2024), within-group shifts to mixotrophy, delayed responses to thermal history (Anderson et al., 2025; Wolf et al., 2024) and nonlinear temperature responses of particulate organic matter and trophic groups (Chen et al., 2015; Wang et al., 2019).

In conclusion, the biological mechanisms proposed here motivate future research vessel campaigns and mesocosm experiments to explicitly manipulate PFT interactions, oligotrophic conditions and lysis impacts on emission rates and air-sea physics. Such experiments still remain scarce, often focusing on single species (i.e. pseudo-axenic cultures) such as the coccolithophore *Emiliania huxleyi* (O'Dowd et al., 2015) or diatoms like *Thalassiosira pseudonana* or *Nitzschia closterium* (Alpert et al., 2015; Sellegri et al., 2021). Accordingly, mesocosm studies have yet to completely capture the role of fully resolved PFT assemblages and biology interactome (Martínez-Pérez et al., 2024) in marine organic aerosols formation, and to explicitly resolve non-linear temperature-biology interactions and realistic wave breaking conditions (Anderson et al., 2025; Liu et al., 2024; Sellegri et al., 2024).

Data availability. The codes supporting the analyses presented in this study will be made openly available on https://doi.org/10.5281/zenodo.20155093 (Chevassus, 2026). The observational time series from the Mace Head Atmospheric Research Station are available from the corresponding author upon request, with a later release planned on EBAS. Phytoplankton functional type fields are available from the AIGD-PFT dataset (Zhang et al., 2024a) while global 9 km gap-filled chl-*a* and suspended particulate matter (SPM) were retrieved from ftp://ftp.star.nesdis.noaa.gov/pub/socd1/mecb/coastwatch/viirs/science/L3/global (last access: 20 February 2026). Gap-filled satellite particulate organic carbon (POC) fields are available from Zhang et al. (2024b). Surface nitrate, phosphate and silicate from the PISCES-based Global Ocean Biogeochemistry Hindcast can be accessed from the Copernicus Marine Service GLOBAL_MULTIYEAR_BGC_001_029 dataset (https://doi.org/10.48670/moi-00019, European Union-Copernicus Marine Service, 2018), and micronekton and zooplankton from the GLOBAL_MULTIYEAR_BGC_001_033 dataset (https://doi.org/10.48670/moi-00020, European Union-Copernicus Marine Service, 2021). Meteorological and wave data are available from ERA5 (https://doi.org/10.24381/cds.adbb2d47, Hersbach et al., 2023).

Supplement. The supplement related to this article is available online at https://doi.org/10.5194/acp-26-16719-2026-supplement.

Author contributions. JO, CO'D, and DC designed the research. DC, JO, VM and KNF operated the instruments and verified the raw data processing. EC, VM, DN and JO produced the postprocessed data and figures. JO, CO'D, DC, WX, LC, VM, DS, LL and VP reedited the manuscript. EC wrote the paper with support from all authors, who commented on the paper.

Competing interests. At least one of the (co-)authors is a member of the editorial board of *Atmospheric Chemistry and Physics*. The peer-review process was guided by an independent editor, and the authors also have no other competing interests to declare.

Disclaimer. Publisher's note: Copernicus Publications remains neutral with regard to jurisdictional claims made in the text, published maps, institutional affiliations, or any other geographical representation in this paper. The authors bear the ultimate responsibility for providing appropriate place names. Views expressed in the text are those of the authors and do not necessarily reflect the views of the publisher.

Acknowledgements. This work was supported by Taighde Éireann – Research Ireland under Grant number 22/FFP-A/10611, the Department of the Environment, Climate and Communications, the Environmental Protection Agency (EPA) of Ireland (AC3 network) and the University of Galway College of Science and Engineering Postgraduate Fellowship no. 127407. This work has also received funding from European Union's Horizon Europe Research and Innovation programme under HORIZON-CL5-2022-D1-02 (grant no. 101081430 – PARIS).

Financial support. This research has been supported by the Research Ireland (grant no. 22/FFP-A/10611). This work has also received funding from European Union's Horizon Europe Research and Innovation programme under HORIZON-CL5-2022-D1-02 (grant no. 20 101081430 – PARIS).

Review statement. This paper was edited by Radovan Krejci and reviewed by Sanjeev Dasari and one anonymous referee.

References

Albernhe, S., Gorgues, T., Lehodey, P., Menkes, C., and Titaud, O.: Magon De La Giclais, S., and Conchon, A.: Global characterization of modelled micronekton in biophysically defined provinces, Prog. Oceanogr., 229, 103370, https://doi.org/10.1016/j.pocean.2024.103370, 2024.

Alpert, P. A., Kilthau, W. P., Bothe, D. W., Radway, J. C., Aller, J. Y., and Knopf, D. A.: The influence of marine microbial activities on aerosol production: A laboratory mesocosm study, J. Geophys. Res.-Atmos., 120, 8841–8860, https://doi.org/10.1002/2015JD023469, 2015.

Alsante, A. N., Thornton, D. C. O., Brooks, S. D., Mirrielees, J. A., Wilbourn, E. K., Matthews, B. H., Diaz, B. P., and Bidle, K. D.: Effect of viral infection on the ice nucleation efficiency of marine coccolithophores, Aerosol Sci. Technol., 59, 195–213, https://doi.org/10.1080/02786826.2024.2420675, 2025.

Anderson, D. M., Fey, S. B., Meier, H. S., Vasseur, D. A., and Kremer, C. T.: Nutrient storage links past thermal exposure to current performance in phytoplankton, P. Natl. Acad. Sci. USA, 122, e2418108122, https://doi.org/10.1073/pnas.2418108122, 2025.

Aumont, O., Ethé, C., Tagliabue, A., Bopp, L., and Gehlen, M.: PISCES-v2: an ocean biogeochemical model for carbon and ecosystem studies, Geosci. Model Dev., 8, 2465–2513, https://doi.org/10.5194/gmd-8-2465-2015, 2015.

Bar-On, Y. M. and Milo, R.: The Biomass Composition of the Oceans: A Blueprint of Our Blue Planet, Cell, 179, 1451–1454, https://doi.org/10.1016/j.cell.2019.11.018, 2019.

Beaupré, S. R., Kieber, D. J., Keene, W. C., Long, M. S., Maben, J. R., Lu, X., Zhu, Y., Frossard, A. A., Kinsey, J. D., Duplessis, P., Chang, R. Y.-W., and Bisgrove, J.: Oceanic efflux of ancient marine dissolved organic carbon in primary marine aerosol, Sci. Adv., 5, eaax6535, https://doi.org/10.1126/sciadv.aax6535, 2019.

Becker, K. W., Devresse, Q., Prieto-Mollar, X., Hinrichs, K.-U., and Engel, A.: Mixed-layer lipidomes suggest offshore transport of energy-rich and essential lipids by cyclonic eddies, Commun. Earth Environ., 6, 179, https://doi.org/10.1038/s43247-025-02152-0, 2025.

Behrenfeld, M. J., Moore, R. H., Hostetler, C. A., Graff, J., Gaube, P., Russell, L. M., Chen, G., Doney, S. C., Giovannoni, S., Liu, H., Proctor, C., Bolaños, L. M., Baetge, N., Davie-Martin, C., Westberry, T. K., Bates, T. S., Bell, T. G., Bidle, K. D., Boss, E. S., Brooks, S. D., Cairns, B., Carlson, C., Halsey, K., Harvey, E. L., Hu, C., Karp-Boss, L., Kleb, M., Menden-Deuer, S., Morison, F., Quinn, P. K., Scarino, A. J., Anderson, B., Chowdhary, J., Crosbie, E., Ferrare, R., Hair, J. W., Hu, Y., Janz, S., Redemann, J., Saltzman, E., Shook, M., Siegel, D. A., Wisthaler, A., Martin, M. Y., and Ziemba, L.: The North Atlantic Aerosol and Marine Ecosystem Study (NAAMES): Science Motive and Mission Overview, Front. Mar. Sci., 6, 122, https://doi.org/10.3389/fmars.2019.00122, 2019.

Bi, Y., Wang, F., and Zhang, W.: Omics Analysis for Dinoflagellates Biology Research, Microorganisms, 7, 288, https://doi.org/10.3390/microorganisms7090288, 2019.

Bolaños, L. M., Choi, C. J., Worden, A. Z., Baetge, N., Carlson, C. A., and Giovannoni, S.: Seasonality of the Microbial Community Composition in the North Atlantic, Front. Mar. Sci., 8, 624164, https://doi.org/10.3389/fmars.2021.624164, 2021.

Brockmann, J. E.: Aerosol Transport in Sampling Lines and Inlets, in: Aerosol Measurement, edited by: Kulkarni, P., Baron, P. A., and Willeke, K., Wiley, 68–105, https://doi.org/10.1002/9781118001684.ch6, 2011.

Brotas, V., Tarran, G. A., Veloso, V., Brewin, R. J. W., Woodward, E. M. S., Airs, R., Beltran, C., Ferreira, A., and Groom, S. B.: Complementary Approaches to Assess Phytoplankton Groups and Size Classes on a Long Transect in the Atlantic Ocean, Front. Mar. Sci., 8, 682621, https://doi.org/10.3389/fmars.2021.682621, 2022.

Bullock, H. A., Luo, H., and Whitman, W. B.: Evolution of Dimethylsulfoniopropionate Metabolism in Marine Phytoplankton and Bacteria, Front. Microbiol., 8, https://doi.org/10.3389/fmicb.2017.00637, 2017.

Burrows, S. M., Easter, R. C., Liu, X., Ma, P.-L., Wang, H., Elliott, S. M., Singh, B., Zhang, K., and Rasch, P. J.: OCEANFILMS (Organic Compounds from Ecosystems to Aerosols: Natural Films and Interfaces via Langmuir Molecular Surfactants) sea spray organic aerosol emissions – implementation in a global climate model and impacts on clouds, Atmos. Chem. Phys., 22, 5223–5251, https://doi.org/10.5194/acp-22-5223-2022, 2022.

Corbin, J. C., Othman, A., Allan, J. D., Worsnop, D. R., Haskins, J. D., Sierau, B., Lohmann, U., and Mensah, A. A.: Peak-fitting and integration imprecision in the Aerodyne aerosol mass spectrometer: effects of mass accuracy on location-constrained fits, Atmos. Meas. Tech., 8, 4615–4636, https://doi.org/10.5194/amt-8-4615-2015, 2015.

C3S: ERA5 hourly data on single levels from 1940 to present, Copernicus Climate Change Service (C3S) Climate Data Store (CDS), https://doi.org/10.24381/CDS.ADBB2D47, 2018.

Cala, B. A., Archer-Nicholls, S., Weber, J., Abraham, N. L., Griffiths, P. T., Jacob, L., Shin, Y. M., Revell, L. E., Woodhouse, M., and Archibald, A. T.: Development, intercomparison, and evaluation of an improved mechanism for the oxidation of dimethyl sulfide in the UKCA model, Atmos. Chem. Phys., 23, 14735–14760, https://doi.org/10.5194/acp-23-14735-2023, 2023.

Callaghan, A., De Leeuw, G., Cohen, L., and O'Dowd, C. D.: Relationship of oceanic whitecap coverage to wind speed and wind history, Geophys. Res. Lett., 35, 2008GL036165, https://doi.org/10.1029/2008GL036165, 2008.

Callaghan, A. H., Stokes, M. D., and Deane, G. B.: The effect of water temperature on air entrainment, bubble plumes, and surface foam in a laboratory breaking-wave analog, J. Geophys. Res.-Oceans, 119, 7463–7482, https://doi.org/10.1002/2014JC010351, 2014.

Campbell, J. W.: The lognormal distribution as a model for bio-optical variability in the sea, J. Geophys. Res., 100, 13237–13254, https://doi.org/10.1029/95JC00458, 1995.

Canonaco, F., Crippa, M., Slowik, J. G., Baltensperger, U., and Prévôt, A. S. H.: SoFi, an IGOR-based interface for the efficient use of the generalized multilinear engine (ME-2) for the source apportionment: ME-2 application to aerosol mass spectrometer data, Atmos. Meas. Tech., 6, 3649–3661, https://doi.org/10.5194/amt-6-3649-2013, 2013.

Chen, C.-S., Anaya, J. M., Chen, E. Y.-T., Farr, E., and Chin, W.-C.: Ocean Warming–Acidification Synergism Undermines Dissolved Organic Matter Assembly, PLoS ONE, 10, e0118300, https://doi.org/10.1371/journal.pone.0118300, 2015.

Cheng, Y., Hui, Y., McAleer, M., and Wong, W.-K.: Spurious Relationships for Nearly Non-Stationary Series, Journal of Risk and Financial Management, 14, 366, https://doi.org/10.3390/jrfm14080366, 2021.

Chevassus, E.: Marine Organic Aerosol Reflects Ecosystem Variability from Phytoplankton Functional Types to Micronekton, Zenodo [code], https://doi.org/10.5281/zenodo.20155093, 2026.

Chevassus, E., Fossum, K. N., Ceburnis, D., Lei, L., Lin, C., Xu, W., O'Dowd, C., and Ovadnevaite, J.: Marine organic aerosol at Mace Head: effects from phytoplankton and source region variability, Atmos. Chem. Phys., 25, 4107–4129, https://doi.org/10.5194/acp-25-4107-2025, 2025.

Cifuentes-Lorenzen, A., Zappa, C. J., Randolph, K., and Edson, J. B.: Scaling the Bubble Penetration Depth in the Ocean, J. Geophys. Res.-Oceans, 128, e2022JC019582, https://doi.org/10.1029/2022JC019582, 2023.

Collins, D. B., Bertram, T. H., Sultana, C. M., Lee, C., Axson, J. L., and Prather, K. A.: Phytoplankton blooms weakly influence the cloud forming ability of sea spray aerosol: CCN From Algae Bloom Microcosms, Geophys. Res. Lett., 43, 9975–9983, https://doi.org/10.1002/2016GL069922, 2016.

Crespi, A., Bernardoni, V., Calzolai, G., Lucarelli, F., Nava, S., Valli, G., and Vecchi, R.: Implementing constrained multi-time approach with bootstrap analysis in ME-2: An application to PM2.5 data from Florence (Italy), Sci. Total Environ., 541, 502–511, https://doi.org/10.1016/j.scitotenv.2015.08.159, 2016.

Crocker, D. R., Hernandez, R. E., Huang, H. D., Pendergraft, M. A., Cao, R., Dai, J., Morris, C. K., Deane, G. B., Prather, K. A., and Thiemens, M. H.: Biological Influence on δ^{13} C and Organic Composition of Nascent Sea Spray Aerosol, ACS Earth Space Chem., 4, 1686–1699, https://doi.org/10.1021/acsearthspacechem.0c00072, 2020.

Czerski, H., Brooks, I. M., Gunn, S., Pascal, R., Matei, A., and Blomquist, B.: Ocean bubbles under high wind conditions – Part 1: Bubble distribution and development, Ocean Sci., 18, 565–586, https://doi.org/10.5194/os-18-565-2022, 2022.

Dacey, J. W. and Wakeham, S. G.: Oceanic dimethylsulfide: production during zooplankton grazing on phytoplankton, Science, 233, 1314–1316, https://doi.org/10.1126/science.233.4770.1314, 1986.

Dall'Osto, M., Vaqué, D., Sotomayor-Garcia, A., Cabrera-Brufau, M., Estrada, M., Buchaca, T., Soler, M., Nunes, S., Zeppenfeld, S., Van Pinxteren, M., Herrmann, H., Wex, H., Rinaldi, M., Paglione, M., Beddows, D. C. S., Harrison, R. M., and Berdalet, E.: Sea Ice Microbiota in the Antarctic Peninsula Modulates Cloud-Relevant Sea Spray Aerosol Production, Front. Mar. Sci., 9, 827061, https://doi.org/10.3389/fmars.2022.827061, 2022.

Dall'Osto, M., Schmidt, K., Campbell, R. G., Nomura, D., Park, J., Yoon, Y. J., and Park, J.: Zooplankton grazing increases atmospheric primary aerosol production in the high Arctic, Elem. Sci. Anth., 13, 00078, https://doi.org/10.1525/elementa.2024.00078, 2025.

Dani, K. G. S. and Loreto, F.: Trade-Off Between Dimethyl Sulfide and Isoprene Emissions from Marine Phytoplankton, Trends Plant Sci., 22, 361–372, https://doi.org/10.1016/j.tplants.2017.01.006, 2017.

DeCarlo, P. F., Kimmel, J. R., Trimborn, A., Northway, M. J., Jayne, J. T., Aiken, A. C., Gonin, M., Fuhrer, K., Horvath, T., Docherty, K. S., Worsnop, D. R., and Jimenez, J. L.: Field-Deployable, High-Resolution, Time-of-Flight Aerosol Mass Spectrometer, Anal. Chem., 78, 8281–8289, https://doi.org/10.1021/ac061249n, 2006.

Deike, L., Reichl, B. G., and Paulot, F.: A Mechanistic Sea Spray Generation Function Based on the Sea State and the Physics of Bubble Bursting, AGU Advances, 3, e2022AV000750, https://doi.org/10.1029/2022AV000750, 2022.

Drewnick, F., Hings, S. S., Alfarra, M. R., Prevot, A. S. H., and Borrmann, S.: Aerosol quantification with the Aerodyne Aerosol Mass Spectrometer: detection limits and ionizer background effects, Atmos. Meas. Tech., 2, 33–46, https://doi.org/10.5194/amt-2-33-2009, 2009.

Duhamel, S., Kim, E., Sprung, B., and Anderson, O. R.: Small pigmented eukaryotes play a major role in carbon cycling in the P-depleted western subtropical North Atlantic, which may be supported by mixotrophy, Limnol. Oceanogr., 64, 2424–2440, https://doi.org/10.1002/lno.11193, 2019.

Efron, B.: Bootstrap Methods: Another Look at the Jackknife, Ann. Stat., 7, 1–26, https://doi.org/10.1214/aos/1176344552, 1979.

Eickhoff, L., Bayer-Giraldi, M., Reicher, N., Rudich, Y., and Koop, T.: Ice nucleating properties of the sea ice diatom *Fragilar-*

iopsis cylindrus and its exudates, Biogeosciences, 20, 1–14, https://doi.org/10.5194/bg-20-1-2023, 2023.

Eigemann, F., Tait, K., Temperton, B., and Hellweger, F. L.: Internal carbon recycling by heterotrophic prokaryotes compensates for mismatches between phytoplankton production and heterotrophic consumption, ISME J., 18, wrae103, https://doi.org/10.1093/ismejo/wrae103, 2024.

European Union-Copernicus Marine Service: Global ocean biogeochemistry hindcast, [data set], https://doi.org/10.48670/MOI-00019, 2018.

European Union-Copernicus Marine Service: Global ocean low and mid trophic levels biomass content hindcast, [data set], https://doi.org/10.48670/MOI-00020, 2021.

European Union-Copernicus Marine Service: Global ocean low and mid trophic levels biomass content hindcast, Mercator Ocean International [data set], https://doi.org/10.48670/MOI-00020, 2021.

Fiddes, S. L., Woodhouse, M. T., Nicholls, Z., Lane, T. P., and Schofield, R.: Cloud, precipitation and radiation responses to large perturbations in global dimethyl sulfide, Atmos. Chem. Phys., 18, 10177–10198, https://doi.org/10.5194/acp-18-10177-2018, 2018.

Flynn, K. J., Kimmance, S. A., Clark, D. R., Mitra, A., Polimene, L., and Wilson, W. H.: Modelling the Effects of Traits and Abiotic Factors on Viral Lysis in Phytoplankton, Front. Mar. Sci., 8, 667184, https://doi.org/10.3389/fmars.2021.667184, 2021.

Forster, P. M., Smith, C. J., Walsh, T., Lamb, W. F., Lamboll, R., Hauser, M., Ribes, A., Rosen, D., Gillett, N., Palmer, M. D., Rogelj, J., von Schuckmann, K., Seneviratne, S. I., Trewin, B., Zhang, X., Allen, M., Andrew, R., Birt, A., Borger, A., Boyer, T., Broersma, J. A., Cheng, L., Dentener, F., Friedlingstein, P., Gutiérrez, J. M., Gütschow, J., Hall, B., Ishii, M., Jenkins, S., Lan, X., Lee, J.-Y., Morice, C., Kadow, C., Kennedy, J., Killick, R., Minx, J. C., Naik, V., Peters, G. P., Pirani, A., Pongratz, J., Schleussner, C.-F., Szopa, S., Thorne, P., Rohde, R., Rojas Corradi, M., Schumacher, D., Vose, R., Zickfeld, K., Masson-Delmotte, V., and Zhai, P.: Indicators of Global Climate Change 2022: annual update of large-scale indicators of the state of the climate system and human influence, Earth Syst. Sci. Data, 15, 2295–2327, https://doi.org/10.5194/essd-15-2295-2023, 2023.

Fossum, K. N., Lin, C., O'Sullivan, N., Lei, L., Hellebust, S., Ceburnis, D., Afzal, A., Tremper, A., Green, D., Jain, S., Byčenkienė, S., O'Dowd, C., Wenger, J., and Ovadnevaite, J.: Two distinct ship emission profiles for organic-sulfate source apportionment of PM in sulfur emission control areas, Atmos. Chem. Phys., 24, 10815–10831, https://doi.org/10.5194/acp-24-10815-2024, 2024.

Freney, E., Sellegri, K., Nicosia, A., Williams, L. R., Rinaldi, M., Trueblood, J. T., Prévôt, A. S. H., Thyssen, M., Grégori, G., Haëntjens, N., Dinasquet, J., Obernosterer, I., Van Wambeke, F., Engel, A., Zäncker, B., Desboeufs, K., Asmi, E., Timonen, H., and Guieu, C.: Mediterranean nascent sea spray organic aerosol and relationships with seawater biogeochemistry, Atmos. Chem. Phys., 21, 10625–10641, https://doi.org/10.5194/acp-21-10625-2021, 2021.

Fulton, J. M., Fredricks, H. F., Bidle, K. D., Vardi, A., Kendrick, B. J., DiTullio, G. R., and Van Mooy, B. A. S.: Novel molecular determinants of viral susceptibility and resistance in the lipidome of *E miliania huxleyi*, Environ. Microbiol., 16, 1137–1149, https://doi.org/10.1111/1462-2920.12358, 2014.

Fung, K. M., Heald, C. L., Kroll, J. H., Wang, S., Jo, D. S., Gettelman, A., Lu, Z., Liu, X., Zaveri, R. A., Apel, E. C., Blake, D. R., Jimenez, J.-L., Campuzano-Jost, P., Veres, P. R., Bates, T. S., Shilling, J. E., and Zawadowicz, M.: Exploring dimethyl sulfide (DMS) oxidation and implications for global aerosol radiative forcing, Atmos. Chem. Phys., 22, 1549–1573, https://doi.org/10.5194/acp-22-1549-2022, 2022.

Gamage, D. K., Hasenecz, E., Dorcé, G. P., Mayer, K. J., Sauer, J. S., Lee, C., Prather, K. A., and Stone, E. A.: Molecular Characterization of Nascent and Aged Sea Spray Aerosol, ACS Earth Space Chem., acsearthspacechem.4c00412, https://doi.org/10.1021/acsearthspacechem.4c00412, 2025.

Gangrade, S. and Mangolte, I.: Patchiness of plankton communities at fronts explained by Lagrangian history of upwelled water parcels, Limnol. Oceanogr., 69, 2123–2137, https://doi.org/10.1002/lno.12654, 2024.

Giannerini, S. and Goracci, G.: Entropy-Based Tests for Complex Dependence in Economic and Financial Time Series with the R Package tseriesEntropy, Mathematics, 11, 757, https://doi.org/10.3390/math11030757, 2023.

Goss, M. B. and Kroll, J. H.: Chamber studies of OH + dimethyl sulfoxide and dimethyl disulfide: insights into the dimethyl sulfide oxidation mechanism, Atmos. Chem. Phys., 24, 1299–1314, https://doi.org/10.5194/acp-24-1299-2024, 2024.

Gray, P. C., Savelyev, I., Cassar, N., Lévy, M., Boss, E., Lehahn, Y., Bourdin, G., Thompson, K. A., Windle, A., Gronniger, J., Floge, S., Hunt, D. E., Silsbe, G., Johnson, Z. I., and Johnston, D. W.: Evidence for Kilometer-Scale Biophysical Features at the Gulf Stream Front, J. Geophys. Res.-Oceans, 129, e2023JC020526, https://doi.org/10.1029/2023JC020526, 2024.

Gu, W., Xie, Z., Wei, Z., Chen, A., Jiang, B., Yue, F., and Yu, X.: Marine Fresh Carbon Pool Dominates Summer Carbonaceous Aerosols Over Arctic Ocean, J. Geophys. Res.-Atmos., 128, e2022JD037692, https://doi.org/10.1029/2022JD037692, 2023.

Guadayol, Ò., Mendonca, T., Segura-Noguera, M., Wright, A. J., Tassieri, M., and Humphries, S.: Microrheology reveals microscale viscosity gradients in planktonic systems, P. Natl. Acad. Sci. USA, 118, e2011389118, https://doi.org/10.1073/pnas.2011389118, 2021.

Hansell, D. A., Romera-Castillo, C., and Lopez, C. N.: Dynamics of dissolved organic carbon in the global ocean, in: Biogeochemistry of Marine Dissolved Organic Matter, Elsevier, 769–802, https://doi.org/10.1016/B978-0-443-13858-4.00004-6, 2024.

Heal, K. R., Durham, B. P., Boysen, A. K., Carlson, L. T., Qin, W., Ribalet, F., White, A. E., Bundy, R. M., Armbrust, E. V., and Ingalls, A. E.: Marine Community Metabolomes Carry Fingerprints of Phytoplankton Community Composition, mSystems, 6, e01334-20, https://doi.org/10.1128/mSystems.01334-20, 2021.

Hernández-León, S.: The biological carbon pump, diel vertical migration, and carbon dioxide removal, iScience, 26, 107835, https://doi.org/10.1016/j.isci.2023.107835, 2023.

Hersbach, H., Bell, B., Berrisford, P., Biavati, G., Horányi, A., Muñoz Sabater, J., Nicolas, J., Peubey, C., Radu, R., Rozum, I., Schepers, D., Simmons, A., Soci, C., Dee, D., and Thépaut, J.-N.: ERA5 hourly data on single levels from 1940 to present, Copernicus Climate Change Service (C3S) Climate Data Store (CDS) [data set], https://doi.org/10.24381/cds.adbb2d47, 2023.

Hodshire, A. L., Campuzano-Jost, P., Kodros, J. K., Croft, B., Nault, B. A., Schroder, J. C., Jimenez, J. L., and Pierce, J. R.: The potential role of methanesulfonic acid (MSA) in aerosol formation and growth and the associated radiative forcings, Atmos. Chem. Phys., 19, 3137–3160, https://doi.org/10.5194/acp-19-3137-2019, 2019.

Holm, H. C., Fredricks, H. F., Bent, S. M., Lowenstein, D. P., Ossolinski, J. E., Becker, K. W., Johnson, W. M., Schrage, K., and Van Mooy, B. A. S.: Global ocean lipidomes show a universal relationship between temperature and lipid unsaturation, Science, 376, 1487–1491, https://doi.org/10.1126/science.abn7455, 2022.

Hong, Z., Long, D., Shan, K., Zhang, J.-M., Woolway, R. I., Liu, M., Mann, M. E., and Fang, H.: Declining ocean greenness and phytoplankton blooms in low to mid-latitudes under a warming climate, Sci. Adv., 11, eadx4857, https://doi.org/10.1126/sciadv.adx4857, 2025.

Hu, J., Li, J., Tsona Tchinda, N., Song, Y., Xu, M., Li, K., and Du, L.: Underestimated role of sea surface temperature in sea spray aerosol formation and climate effects, npj Clim. Atmos. Sci., 7, 273, https://doi.org/10.1038/s41612-024-00823-x, 2024.

Hulswar, S., Simó, R., Galí, M., Bell, T. G., Lana, A., Inamdar, S., Halloran, P. R., Manville, G., and Mahajan, A. S.: Third revision of the global surface seawater dimethyl sulfide climatology (DMS-Rev3), Earth Syst. Sci. Data, 14, 2963–2987, https://doi.org/10.5194/essd-14-2963-2022, 2022.

Ickes, L., Porter, G. C. E., Wagner, R., Adams, M. P., Bierbauer, S., Bertram, A. K., Bilde, M., Christiansen, S., Ekman, A. M. L., Gorokhova, E., Höhler, K., Kiselev, A. A., Leck, C., Möhler, O., Murray, B. J., Schiebel, T., Ullrich, R., and Salter, M. E.: The ice-nucleating activity of Arctic sea surface microlayer samples and marine algal cultures, Atmos. Chem. Phys., 20, 11089–11117, https://doi.org/10.5194/acp-20-11089-2020, 2020.

Jackson, R. and Gabric, A.: Climate Change Impacts on the Marine Cycling of Biogenic Sulfur: A Review, Microorganisms, 10, 1581, https://doi.org/10.3390/microorganisms10081581, 2022.

Jang, E., Park, K.-T., Yoon, Y. J., Kim, T.-W., Hong, S.-B., Becagli, S., Traversi, R., Kim, J., and Gim, Y.: New particle formation events observed at the King Sejong Station, Antarctic Peninsula – Part 2: Link with the oceanic biological activities, Atmos. Chem. Phys., 19, 7595–7608, https://doi.org/10.5194/acp-19-7595-2019, 2019.

Jiang, X., Rotily, L., Villermaux, E., and Wang, X.: Submicron drops from flapping bursting bubbles, P. Natl. Acad. Sci. USA, 119, e2112924119, https://doi.org/10.1073/pnas.2112924119, 2022.

Jung, J., Hong, S.-B., Chen, M., Hur, J., Jiao, L., Lee, Y., Park, K., Hahm, D., Choi, J.-O., Yang, E. J., Park, J., Kim, T.-W., and Lee, S.: Characteristics of methanesulfonic acid, non-sea-salt sulfate and organic carbon aerosols over the Amundsen Sea, Antarctica, Atmos. Chem. Phys., 20, 5405–5424, https://doi.org/10.5194/acp-20-5405-2020, 2020.

Kaluarachchi, C. P., Or, V. W., Lan, Y., Hasenecz, E. S., Kim, D., Madawala, C. K., Dorcé, G. P., Mayer, K. J., Sauer, J. S., Lee, C., Cappa, C. D., Bertram, T. H., Stone, E. A., Prather, K. A., Grassian, V. H., and Tivanski, A. V.: Effects of Atmospheric Aging Processes on Nascent Sea Spray Aerosol Physicochemical Properties, ACS Earth Space Chem., 6, 2732–2744, https://doi.org/10.1021/acsearthspacechem.2c00258, 2022.

Kawana, K., Miyazaki, Y., Omori, Y., Tanimoto, H., Kagami, S., Suzuki, K., Yamashita, Y., Nishioka, J., Deng, Y., Yai, H., and Mochida, M.: Number-Size Distribution and CCN Activity of Atmospheric Aerosols in the Western North Pacific During Spring Pre-Bloom Period: Influences of Terrestrial and Marine Sources, J. Geophys. Res.-Atmos., 127, e2022JD036690, https://doi.org/10.1029/2022JD036690, 2022.

Killick, R., Beaulieu, C., Taylor, S., and Hullait, H.: EnvCpt: Detection of Structural Changes in Climate and Environment Time Series, https://cran.r-project.org/web/packages/EnvCpt/index.html (last access: 12 February 2026), 2018.

Klawonn, I., Van Den Wyngaert, S., Parada, A. E., Arandia-Gorostidi, N., Whitehouse, M. J., Grossart, H.-P., and Dekas, A. E.: Characterizing the "fungal shunt": Parasitic fungi on diatoms affect carbon flow and bacterial communities in aquatic microbial food webs, P. Natl. Acad. Sci. USA, 118, e2102225118, https://doi.org/10.1073/pnas.2102225118, 2021.

Kranzler, C. F., Krause, J. W., Brzezinski, M. A., Edwards, B. R., Biggs, W. P., Maniscalco, M., McCrow, J. P., Van Mooy, B. A. S., Bidle, K. D., Allen, A. E., and Thamatrakoln, K.: Silicon limitation facilitates virus infection and mortality of marine diatoms, Nat. Microbiol., 4, 1790–1797, https://doi.org/10.1038/s41564-019-0502-x, 2019.

Krisch, S., Browning, T. J., Graeve, M., Ludwichowski, K.-U., Lodeiro, P., Hopwood, M. J., Roig, S., Yong, J.-C., Kanzow, T., and Achterberg, E. P.: The influence of Arctic Fe and Atlantic fixed N on summertime primary production in Fram Strait, North Greenland Sea, Sci. Rep., 10, 15230, https://doi.org/10.1038/s41598-020-72100-9, 2020.

Kruskopf, M. and Flynn, K. J.: Chlorophyll content and fluorescence responses cannot be used to gauge reliably phytoplankton biomass, nutrient status or growth rate, New Phytol., 169, 525–536, https://doi.org/10.1111/j.1469-8137.2005.01601.x, 2006.

Kuhlisch, C., Schleyer, G., Shahaf, N., Vincent, F., Schatz, D., and Vardi, A.: Viral infection of algal blooms leaves a unique metabolic footprint on the dissolved organic matter in the ocean, Sci. Adv., 7, eabf4680, https://doi.org/10.1126/sciadv.abf4680, 2021.

Law, C. S. and Miller, L. A.: The air-sea interface in a changing climate: Research advances and future directions, Elem. Sci. Anth., 13, 00022, https://doi.org/10.1525/elementa.2025.00022, 2025.

Lawler, M. J., Schill, G. P., Brock, C. A., Froyd, K. D., Williamson, C., Kupc, A., and Murphy, D. M.: Sea Spray Aerosol Over the Remote Oceans Has Low Organic Content, AGU Adv., 5, e2024AV001215, https://doi.org/10.1029/2024AV001215, 2024.

Le Gland, G., Masdeu-Navarro, M., Galí, M., Vallina, S. M., Gralka, M., Vincent, F., Cordero, O., Vardi, A., and Simó, R.: Biological sources and sinks of dimethylsulfide disentangled by an induced bloom experiment and a numerical model, Limnol. Oceanogr., 69, 140–157, https://doi.org/10.1002/lno.12470, 2024.

Leibensperger III, R. J., Hamlin, J. D., Herbst, J. K., Harb, C., Kimble, K. A., Andreae, M. O., Lee, C., Sandstrom, G., Stokes, M. D., Deane, G. B., and Prather, K. A.: Sea surface warming suppresses primary sea spray aerosol number production, Atmos. Chem. Phys., 26, 12211–12229, https://doi.org/10.5194/acp-26-12211-2026, 2026.

Leon-Marcos, A., Zeising, M., van Pinxteren, M., Zeppenfeld, S., Bracher, A., Barbaro, E., Engel, A., Feltracco, M., Tegen, I., and Heinold, B.: Modelling emission and transport of key compo-

nents of primary marine organic aerosol using the global aerosol–climate model ECHAM6.3–HAM2.3, Geosci. Model Dev., 18, 4183–4213, https://doi.org/10.5194/gmd-18-4183-2025, 2025.

Lima-Mendez, G., Faust, K., Henry, N., Decelle, J., Colin, S., Carcillo, F., Chaffron, S., Ignacio-Espinosa, J. C., Roux, S., Vincent, F., Bittner, L., Darzi, Y., Wang, J., Audic, S., Berline, L., Bontempi, G., Cabello, A. M., Coppola, L., Cornejo-Castillo, F. M., d'Ovidio, F., De Meester, L., Ferrera, I., Garet-Delmas, M.-J., Guidi, L., Lara, E., Pesant, S., Royo-Llonch, M., Salazar, G., Sánchez, P., Sebastian, M., Souffreau, C., Dimier, C., Picheral, M., Searson, S., Kandels-Lewis, S., Tara Oceans coordinators, Gorsky, G., Not, F., Ogata, H., Speich, S., Stemmann, L., Weissenbach, J., Wincker, P., Acinas, S. G., Sunagawa, S., Bork, P., Sullivan, M. B., Karsenti, E., Bowler, C., De Vargas, C., and Raes, J.: Determinants of community structure in the global plankton interactome, Science, 348, 1262073, https://doi.org/10.1126/science.1262073, 2015.

Liu, C., Li, H., Zheng, H., Wang, G., Qin, X., Chen, J., Zhou, S., Lu, D., Liang, G., Song, X., Duan, Y., Liu, J., Huang, K., and Deng, C.: Ocean Emission Pathway and Secondary Formation Mechanism of Aminiums Over the Chinese Marginal Sea, J. Geophys. Res.-Atmos., 127, e2022JD037805, https://doi.org/10.1029/2022JD037805, 2022.

Liu, W., Holm, H. C., Lipp, J. S., Fredricks, H. F., Van Mooy, B. A. S., and Hinrichs, K.-U.: Unraveling plankton adaptation in global oceans through the untargeted analysis of lipidomes, Sci. Adv., 11, eads4605, https://doi.org/10.1126/sciadv.ads4605, 2025a.

Liu, X. and Wang, M.: Global daily gap-free ocean color products from multi-satellite measurements, Int. J. Appl. Earth Obs., 108, 102714, https://doi.org/10.1016/j.jag.2022.102714, 2022.

Liu, X., Gao, Q., Zhao, F., Jiang, X., Ma, X., Yang, S., Zhu, Y., Wang, Z., Huang, K., Lu, X., and Wang, X.: Sea Surface Temperature: A Key Regulator of Global Perfluoroalkyl Acids Transport across the Sea–Air Interface, Environ. Sci. Technol. Lett., 13, 123–129, https://doi.org/10.1021/acs.estlett.5c01094, 2026.

Liu, Y., Yu, L., Yao, Z., Shen, Y., and Pan, Y.: The effects of turbulence on the growth of three different diatom species, Front. Mar. Sci., 11, 1400798, https://doi.org/10.3389/fmars.2024.1400798, 2024.

Liu, Y., He, Q., Zhan, W., Guo, M., Zheng, Y., Shen, X., and Zhan, H.: Heterogeneity of phytoplankton response to submesoscale processes in the global ocean, Commun. Earth Environ., 6, 386, https://doi.org/10.1038/s43247-025-02365-3, 2025b.

Long, M. S., Keene, W. C., Kieber, D. J., Frossard, A. A., Russell, L. M., Maben, J. R., Kinsey, J. D., Quinn, P. K., and Bates, T. S.: Light-enhanced primary marine aerosol production from biologically productive seawater: Light-Enhanced Marine Aerosol Production, Geophys. Res. Lett., 41, 2661–2670, https://doi.org/10.1002/2014GL059436, 2014.

Longhurst, A. R.: Ecological Geography of the Sea, 2nd edn., Academic Press, https://doi.org/10.1016/B978-0-12-455521-1.X5000-1, 2007.

Lowenstein, D. P., Holm, H. C., Fredricks, H. F., and Van Mooy, B. A. S.: Lipid stoichiometry and biomarkers reflect microbial acclimation and nutrient stress across the Atlantic Ocean, Nat. Commun., https://doi.org/10.1038/s41467-026-79011-9, 2026.

Lu, Z., Qin, G., Zheng, L., Zhang, Y., Huang, L., Zhou, J., Liu, Y., Zheng, M., Hou, E., Song, L., Liu, H., Jiao, N., and Wang, F.: The role of phytoplankton in structuring global oceanic dissolved organic carbon pools, Nat. Commun., 16, 7742, https://doi.org/10.1038/s41467-025-63105-x, 2025.

Ma, X., Coleman, M. L., and Waldbauer, J. R.: Distinct molecular signatures in dissolved organic matter produced by viral lysis of marine cyanobacteria, Environ. Microbiol., 20, 3001–3011, https://doi.org/10.1111/1462-2920.14338, 2018.

Maat, D. and Brussaard, C.: Both phosphorus- and nitrogen limitation constrain viral proliferation in marine phytoplankton, Aquat. Microb. Ecol., 77, 87–97, https://doi.org/10.3354/ame01791, 2016.

Maat, D., Biggs, T., Evans, C., Van Bleijswijk, J., Van Der Wel, N., Dutilh, B., and Brussaard, C.: Characterization and Temperature Dependence of Arctic Micromonas polaris Viruses, Viruses, 9, 134, https://doi.org/10.3390/v9060134, 2017.

Malfatti, F., Lee, C., Tinta, T., Pendergraft, M. A., Celussi, M., Zhou, Y., Sultana, C. M., Rotter, A., Axson, J. L., Collins, D. B., Santander, M. V., Anides Morales, A. L., Aluwihare, L. I., Riemer, N., Grassian, V. H., Azam, F., and Prather, K. A.: Detection of Active Microbial Enzymes in Nascent Sea Spray Aerosol: Implications for Atmospheric Chemistry and Climate, Environ. Sci. Technol. Lett., 6, 171–177, https://doi.org/10.1021/acs.estlett.8b00699, 2019.

Malitsky, S., Ziv, C., Rosenwasser, S., Zheng, S., Schatz, D., Porat, Z., Ben-Dor, S., Aharoni, A., and Vardi, A.: Viral infection of the marine alga *Emiliania huxleyi* triggers lipidome remodeling and induces the production of highly saturated triacylglycerol, New Phytol., 210, 88–96, https://doi.org/10.1111/nph.13852, 2016.

Mansour, K., Decesari, S., Ceburnis, D., Ovadnevaite, J., Russell, L. M., Paglione, M., Poulain, L., Huang, S., O'Dowd, C., and Rinaldi, M.: IPB-MSA&SO_4: a daily 0.25° resolution dataset of in situ-produced biogenic methanesulfonic acid and sulfate over the North Atlantic during 1998–2022 based on machine learning, Earth Syst. Sci. Data, 16, 2717–2740, https://doi.org/10.5194/essd-16-2717-2024, 2024.

Markuszewski, P., Nilsson, E. D., Zinke, J., Mårtensson, E. M., Salter, M., Makuch, P., Kitowska, M., Niedźwiecka-Wróbel, I., Drozdowska, V., Lis, D., Petelski, T., Ferrero, L., and Piskozub, J.: Multi-year gradient measurements of sea spray fluxes over the Baltic Sea and the North Atlantic Ocean, Atmos. Chem. Phys., 24, 11227–11253, https://doi.org/10.5194/acp-24-11227-2024, 2024.

Marsay, C. M., Sanders, R. J., Henson, S. A., Pabortsava, K., Achterberg, E. P., and Lampitt, R. S.: Attenuation of sinking particulate organic carbon flux through the mesopelagic ocean, P. Natl. Acad. Sci. USA, 112, 1089–1094, https://doi.org/10.1073/pnas.1415311112, 2015.

Martínez-Pérez, C., Zweifel, S. T., Pioli, R., and Stocker, R.: Space, the final frontier: The spatial component of phytoplankton–bacterial interactions, Mol. Microbiol., 122, 331–346, https://doi.org/10.1111/mmi.15293, 2024.

Mauritsen, T., Tsushima, Y., Meyssignac, B., Loeb, N. G., Hakuba, M., Pilewskie, P., Cole, J., Suzuki, K., Ackerman, T. P., Allan, R. P., Andrews, T., Bender, F. A. -M., Bloch-Johnson, J., Bodas-Salcedo, A., Brookshaw, A., Ceppi, P., Clerbaux, N., Dessler, A. E., Donohoe, A., Dufresne, J., Eyring, V., Findell, K. L., Gettelman, A., Gristey, J. J., Hawkins, E., Heimbach, P., Hewitt, H. T., Jeevanjee, N., Jones, C., Kang, S. M., Kato, S., Kay, J. E., Klein, S. A., Knutti, R., Kramer, R., Lee, J., McCoy, D. T., Medeiros, B., Megner, L., Modak, A., Ogura, T., Palmer,

M. D., Paynter, D., Quaas, J., Ramanathan, V., Ringer, M., Von Schuckmann, K., Sherwood, S., Stevens, B., Tan, I., Tselioudis, G., Sutton, R., Voigt, A., Watanabe, M., Webb, M. J., Wild, M., and Zelinka, M. D.: Earth's Energy Imbalance More Than Doubled in Recent Decades, AGU Adv., 6, e2024AV001636, https://doi.org/10.1029/2024AV001636, 2025.

McParland, E. L. and Levine, N. M.: The role of differential DMSP production and community composition in predicting variability of global surface DMSP concentrations, Limnol. Oceanogr., 64, 757–773, https://doi.org/10.1002/lno.11076, 2019.

Middlebrook, A. M., Bahreini, R., Jimenez, J. L., and Canagaratna, M. R.: Evaluation of Composition-Dependent Collection Efficiencies for the Aerodyne Aerosol Mass Spectrometer using Field Data, Aerosol Sci. Technol., 46, 258–271, https://doi.org/10.1080/02786826.2011.620041, 2012.

Moallemi, A., Landwehr, S., Robinson, C., Simó, R., Zamanillo, M., Chen, G., Baccarini, A., Schnaiter, M., Henning, S., Modini, R. L., Gysel-Beer, M., and Schmale, J.: Sources, Occurrence and Characteristics of Fluorescent Biological Aerosol Particles Measured Over the Pristine Southern Ocean, J. Geophys. Res.-Atmos., 126, e2021JD034811, https://doi.org/10.1029/2021JD034811, 2021.

Modini, R. L., Russell, L. M., Deane, G. B., and Stokes, M. D.: Effect of soluble surfactant on bubble persistence and bubble-produced aerosol particles, J. Geophys. Res.-Atmos., 118, 1388–1400, https://doi.org/10.1002/jgrd.50186, 2013.

Mojica, K. D. A. and Brussaard, C. P. D.: Marine Viruses and Their Role in Marine Ecosystems and Carbon Cycling, Annu. Rev. Mar. Sci., 18, 351–380, https://doi.org/10.1146/annurev-marine-040324-020244, 2026.

Mojica, K. D. A., Huisman, J., Wilhelm, S. W., and Brussaard, C. P. D.: Latitudinal variation in virus-induced mortality of phytoplankton across the North Atlantic Ocean, ISME J., 10, 500–513, https://doi.org/10.1038/ismej.2015.130, 2016.

Moritz, S. and Bartz-Beielstein, T.: imputeTS: Time Series Missing Value Imputation in R, R J., 9, 207–218, https://doi.org/10.32614/RJ-2017-009, 2017.

Moschos, V., Chevassus, E., Fossum, K., Lei, L., Pernov, J., Humphries, R., Keywood, M., O'Dowd, C., Ceburnis, D., and Ovadnevaite, J.: Rising natural aerosols drive marine radiative forcing as pollution declines, Research Square [preprint], https://doi.org/10.21203/rs.3.rs-8776460/v1, 2026.

Needham, D. M. and Fuhrman, J. A.: Pronounced daily succession of phytoplankton, archaea and bacteria following a spring bloom, Nat. Microbiol., 1, 16005, https://doi.org/10.1038/nmicrobiol.2016.5, 2016.

O'Dowd, C., Ceburnis, D., Ovadnevaite, J., Vaishya, A., Rinaldi, M., and Facchini, M. C.: Do anthropogenic, continental or coastal aerosol sources impact on a marine aerosol signature at Mace Head?, Atmos. Chem. Phys., 14, 10687–10704, https://doi.org/10.5194/acp-14-10687-2014, 2014.

O'Dowd, C., Ceburnis, D., Ovadnevaite, J., Bialek, J., Stengel, D. B., Zacharias, M., Nitschke, U., Connan, S., Rinaldi, M., Fuzzi, S., Decesari, S., Cristina Facchini, M., Marullo, S., Santoleri, R., Dell'Anno, A., Corinaldesi, C., Tangherlini, M., and Danovaro, R.: Connecting marine productivity to sea-spray via nanoscale biological processes: Phytoplankton Dance or Death Disco?, Sci. Rep., 5, 14883, https://doi.org/10.1038/srep14883, 2015.

O'Dowd, C. D., Facchini, M. C., Cavalli, F., Ceburnis, D., Mircea, M., Decesari, S., Fuzzi, S., Yoon, Y. J., and Putaud, J.-P.: Biogenically driven organic contribution to marine aerosol, Nature, 431, 676–680, https://doi.org/10.1038/nature02959, 2004.

Ovadnevaite, J., O'Dowd, C., Dall'Osto, M., Ceburnis, D., Worsnop, D. R., and Berresheim, H.: Detecting high contributions of primary organic matter to marine aerosol: A case study, Geophys. Res. Lett., 38, https://doi.org/10.1029/2010GL046083, 2011a.

Ovadnevaite, J., Ceburnis, D., Martucci, G., Bialek, J., Monahan, C., Rinaldi, M., Facchini, M. C., Berresheim, H., Worsnop, D. R., and O'Dowd, C.: Primary marine organic aerosol: A dichotomy of low hygroscopicity and high CCN activity: MARINE AEROSOL-CLOUD INTERACTIONS, Geophys. Res. Lett., L21806, https://doi.org/10.1029/2011GL048869, 2011b.

Ovadnevaite, J., Manders, A., de Leeuw, G., Ceburnis, D., Monahan, C., Partanen, A.-I., Korhonen, H., and O'Dowd, C. D.: A sea spray aerosol flux parameterization encapsulating wave state, Atmos. Chem. Phys., 14, 1837–1852, https://doi.org/10.5194/acp-14-1837-2014, 2014a.

Ovadnevaite, J., Ceburnis, D., Leinert, S., Dall'Osto, M., Canagaratna, M., O'Doherty, S., Berresheim, H., and O'Dowd, C.: Submicron NE Atlantic marine aerosol chemical composition and abundance: Seasonal trends and air mass categorization: Seasonal Trends of Marine Aerosol, J. Geophys. Res.-Atmos., 119, 11850–11863, https://doi.org/10.1002/2013JD021330, 2014b.

Ovadnevaite, J., Zuend, A., Laaksonen, A., Sanchez, K. J., Roberts, G., Ceburnis, D., Decesari, S., Rinaldi, M., Hodas, N., Facchini, M. C., Seinfeld, J. H., and O'Dowd, C.: Surface tension prevails over solute effect in organic-influenced cloud droplet activation, Nature, 546, 637–641, https://doi.org/10.1038/nature22806, 2017.

Owen, K., Saeki, K., Warren, J. D., Bocconcelli, A., Wiley, D. N., Ohira, S.-I., Bombosch, A., Toda, K., and Zitterbart, D. P.: Natural dimethyl sulfide gradients would lead marine predators to higher prey biomass, Commun. Biol., 4, 149, https://doi.org/10.1038/s42003-021-01668-3, 2021.

Partanen, A.-I., Dunne, E. M., Bergman, T., Laakso, A., Kokkola, H., Ovadnevaite, J., Sogacheva, L., Baisnée, D., Sciare, J., Manders, A., O'Dowd, C., de Leeuw, G., and Korhonen, H.: Global modelling of direct and indirect effects of sea spray aerosol using a source function encapsulating wave state, Atmos. Chem. Phys., 14, 11731–11752, https://doi.org/10.5194/acp-14-11731-2014, 2014.

Pierella Karlusich, J. J., Cosnier, K., Zinger, L., Henry, N., Nef, C., Bernard, G., Scalco, E., Dvorak, E., Tara Oceans Coordinators, Acinas, S. G., Babin, M., Bork, P., Boss, E., Bowler, C., Cochrane, G., De Vargas, C., Gorsky, G., Grimsley, N., Guidi, L., Iudicone, D., Jaillon, O., Kandels, S., Karp-Boss, L., Karsenti, E., Not, F., Ogata, H., Pesant, S., Poulton, N., Sardet, C., Speich, S., Stemmann, L., Sullivan, M. B., Sunagawa, S., Wincker, P., Rocha Jimenez Vieira, F., Delage, E., Chaffron, S., Ovchinnikov, S., Zingone, A., and Bowler, C.: Patterns and drivers of diatom diversity and abundance in the global ocean, Nat. Commun., 16, https://doi.org/10.1038/s41467-025-58027-7, 2025.

Prochaska, J. X. and Frouin, R. J.: On the Peril of Inferring Phytoplankton Properties from Remote-Sensing Observations, arXiv [preprint], https://doi.org/10.48550/ARXIV.2408.06149, 2024, 2024.

Rahlff, J., Stolle, C., Giebel, H.-A., Brinkhoff, T., Ribas-Ribas, M., Hodapp, D., and Wurl, O.: High wind speeds prevent formation of a distinct bacterioneuston community in the sea-surface microlayer, FEMS Microbiol. Ecol., 93, https://doi.org/10.1093/femsec/fix041, 2017.

Ribeiro, C. P. and Mewes, D.: On the effect of liquid temperature upon bubble coalescence, Chem. Eng. Sci., 61, 5704–5716, https://doi.org/10.1016/j.ces.2006.04.043, 2006.

Rosati, B., Isokääntä, S., Christiansen, S., Jensen, M. M., Moosakutty, S. P., Wollesen de Jonge, R., Massling, A., Glasius, M., Elm, J., Virtanen, A., and Bilde, M.: Hygroscopicity and CCN potential of DMS-derived aerosol particles, Atmos. Chem. Phys., 22, 13449–13466, https://doi.org/10.5194/acp-22-13449-2022, 2022.

Rosenwasser, S., Mausz, M. A., Schatz, D., Sheyn, U., Malitsky, S., Aharoni, A., Weinstock, E., Tzfadia, O., Ben-Dor, S., Feldmesser, E., Pohnert, G., and Vardi, A.: Rewiring Host Lipid Metabolism by Large Viruses Determines the Fate of *Emiliania huxleyi*, a Bloom-Forming Alga in the Ocean, Plant Cell, 26, 2689–2707, https://doi.org/10.1105/tpc.114.125641, 2014.

Schreiber, T. and Schmitz, A.: Improved Surrogate Data for Nonlinearity Tests, Phys. Rev. Lett., 77, 635–638, https://doi.org/10.1103/PhysRevLett.77.635, 1996.

Schwier, A. N., Rose, C., Asmi, E., Ebling, A. M., Landing, W. M., Marro, S., Pedrotti, M.-L., Sallon, A., Iuculano, F., Agusti, S., Tsiola, A., Pitta, P., Louis, J., Guieu, C., Gazeau, F., and Sellegri, K.: Primary marine aerosol emissions from the Mediterranean Sea during pre-bloom and oligotrophic conditions: correlations to seawater chlorophyll *a* from a mesocosm study, Atmos. Chem. Phys., 15, 7961–7976, https://doi.org/10.5194/acp-15-7961-2015, 2015.

Schwier, A. N., Sellegri, K., Mas, S., Charrière, B., Pey, J., Rose, C., Temime-Roussel, B., Jaffrezo, J.-L., Parin, D., Picard, D., Ribeiro, M., Roberts, G., Sempéré, R., Marchand, N., and D'Anna, B.: Primary marine aerosol physical flux and chemical composition during a nutrient enrichment experiment in mesocosms in the Mediterranean Sea, Atmos. Chem. Phys., 17, 14645–14660, https://doi.org/10.5194/acp-17-14645-2017, 2017.

Seidel, M., Vemulapalli, S. P. B., Mathieu, D., and Dittmar, T.: Marine Dissolved Organic Matter Shares Thousands of Molecular Formulae Yet Differs Structurally across Major Water Masses, Environ. Sci. Technol., 56, 3758–3769, https://doi.org/10.1021/acs.est.1c04566, 2022.

Sellegri, K., Nicosia, A., Freney, E., Uitz, J., Thyssen, M., Grégori, G., Engel, A., Zäncker, B., Haëntjens, N., Mas, S., Picard, D., Saint-Macary, A., Peltola, M., Rose, C., Trueblood, J., Lefevre, D., D'Anna, B., Desboeufs, K., Meskhidze, N., Guieu, C., and Law, C. S.: Surface ocean microbiota determine cloud precursors, Sci. Rep., 11, 281, https://doi.org/10.1038/s41598-020-78097-5, 2021.

Sellegri, K., Barthelmeß, T., Trueblood, J., Cristi, A., Freney, E., Rose, C., Barr, N., Harvey, M., Safi, K., Deppeler, S., Thompson, K., Dillon, W., Engel, A., and Law, C.: Quantified effect of seawater biogeochemistry on the temperature dependence of sea spray aerosol fluxes, Atmos. Chem. Phys., 23, 12949–12964, https://doi.org/10.5194/acp-23-12949-2023, 2023a.

Sellegri, K., Harvey, M., Peltola, M., Saint-Macary, A., Barthelmeß, T., Rocco, M., Moore, K. A., Cristi, A., Peyrin, F., Barr, N., Labonnote, L., Marriner, A., McGregor, J., Safi, K., Deppeler, S., Archer, S., Dunne, E., Harnwell, J., Delanoe, J., Freney, E., Rose, C., Bazantay, C., Planche, C., Saiz-Lopez, A., Quintanilla-López, J. E., Lebrón-Aguilar, R., Rinaldi, M., Banson, S., Joseph, R., Lupascu, A., Jourdan, O., Mioche, G., Colomb, A., Olivares, G., Querel, R., McDonald, A., Plank, G., Bukosa, B., Dillon, W., Pelon, J., Baray, J.-L., Tridon, F., Donnadieu, F., Szczap, F., Engel, A., DeMott, P. J., and Law, C. S.: Sea2Cloud: From Biogenic Emission Fluxes to Cloud Properties in the Southwest Pacific, B. Am. Meteor. Soc., 104, E1017–E1043, https://doi.org/10.1175/BAMS-D-21-0063.1, 2023b.

Sellegri, K., Simó, R., Wang, B., Alpert, P. A., Altieri, K., Burrows, S., Hopkins, F. E., Koren, I., McCoy, I. L., Ovadnevaite, J., Salter, M., and Schmale, J.: Influence of open ocean biogeochemistry on aerosol and clouds: Recent findings and perspectives, Elem. Sci. Anth., 12, 00058, https://doi.org/10.1525/elementa.2023.00058, 2024.

Shemi, A., Ben-Dor, S., Rotkopf, R., Dym, O., and Vardi, A.: Phylogeny and biogeography of the algal DMS-releasing enzyme in the global ocean, ISME Commun., 3, https://doi.org/10.1038/s43705-023-00280-2, 2023.

Simis, S. G. H., Ruiz-Verdú, A., Domínguez-Gómez, J. A., Peña-Martinez, R., Peters, S. W. M., and Gons, H. J.: Influence of phytoplankton pigment composition on remote sensing of cyanobacterial biomass, Remote Sens. Environ., 106, 414–427, https://doi.org/10.1016/j.rse.2006.09.008, 2007.

Stein, A. F., Draxler, R. R., Rolph, G. D., Stunder, B. J. B., Cohen, M. D., and Ngan, F.: NOAA's HYSPLIT Atmospheric Transport and Dispersion Modeling System, B. Am. Meteor. Soc., 96, 2059–2077, https://doi.org/10.1175/BAMS-D-14-00110.1, 2015.

Taipale, S., Peltomaa, E., and Salmi, P.: Variation in ω-3 and ω-6 Polyunsaturated Fatty Acids Produced by Different Phytoplankton Taxa at Early and Late Growth Phase, Biomolecules, 10, 559, https://doi.org/10.3390/biom10040559, 2020.

Theiler, J., Eubank, S., Longtin, A., Galdrikian, B., and Doyne Farmer, J.: Testing for nonlinearity in time series: the method of surrogate data, Physica D, 58, 77–94, https://doi.org/10.1016/0167-2789(92)90102-S, 1992.

Thibault, H., Ménard, F., Abitbol-Spangaro, J., Poggiale, J.-C., and Martini, S.: Modeling the contribution of micronekton diel vertical migrations to carbon export in the mesopelagic zone, Biogeosciences, 22, 2181–2200, https://doi.org/10.5194/bg-22-2181-2025, 2025.

Thornton, D. C. O.: Dissolved organic matter (DOM) release by phytoplankton in the contemporary and future ocean, Euro. J. Phycol., 49, 20–46, https://doi.org/10.1080/09670262.2013.875596, 2014.

Thornton, D. C. O., Brooks, S. D., Wilbourn, E. K., Mirrielees, J., Alsante, A. N., Gold-Bouchot, G., Whitesell, A., and McFadden, K.: Production of ice-nucleating particles (INPs) by fast-growing phytoplankton, Atmos. Chem. Phys., 23, 12707–12729, https://doi.org/10.5194/acp-23-12707-2023, 2023.

Trueblood, J. V., Nicosia, A., Engel, A., Zäncker, B., Rinaldi, M., Freney, E., Thyssen, M., Obernosterer, I., Dinasquet, J., Belosi, F., Tovar-Sánchez, A., Rodriguez-Romero, A., Santachiara, G., Guieu, C., and Sellegri, K.: A two-component parameterization of marine ice-nucleating particles based on seawater biology and sea spray aerosol measurements in the Mediterranean Sea, At-

mos. Chem. Phys., 21, 4659–4676, https://doi.org/10.5194/acp-21-4659-2021, 2021.

Villermaux, E., Wang, X., and Deike, L.: Bubbles spray aerosols: Certitudes and mysteries, PNAS Nexus, 1, pgac261, https://doi.org/10.1093/pnasnexus/pgac261, 2022.

Wang, J., Curson, A. R. J., Zhou, S., Carrión, O., Liu, J., Vieira, A. R., Walsham, K. S., Monaco, S., Li, C.-Y., Dong, Q.-Y., Wang, Y., Rivera, P. P. L., Wang, X.-D., Zhang, M., Hanwell, L., Wallace, M., Zhu, X.-Y., Leão, P. N., Lea-Smith, D. J., Zhang, Y.-Z., Zhang, X.-H., and Todd, J. D.: Alternative dimethylsulfoniopropionate biosynthesis enzymes in diverse and abundant microorganisms, Nat. Microbiol., 9, 1979–1992, https://doi.org/10.1038/s41564-024-01715-9, 2024.

Wang, Q., Lyu, Z., Omar, S., Cornell, S., Yang, Z., and Montagnes, D. J. S.: Predicting temperature impacts on aquatic productivity: Questioning the metabolic theory of ecology's "canonical" activation energies, Limnol. Oceanogr., 64, 1172–1185, https://doi.org/10.1002/lno.11105, 2019.

Wang, S., Tang, W., Delage, E., Gifford, S., Whitby, H., González, A. G., Eveillard, D., Planquette, H., and Cassar, N.: Investigating the microbial ecology of coastal hotspots of marine nitrogen fixation in the western North Atlantic, Sci. Rep., 11, 5508, https://doi.org/10.1038/s41598-021-84969-1, 2021.

Wenley, J., Currie, K., Lockwood, S., Thomson, B., Baltar, F., and Morales, S. E.: Seasonal Prokaryotic Community Linkages Between Surface and Deep Ocean Water, Front. Mar. Sci., 8, 659641, https://doi.org/10.3389/fmars.2021.659641, 2021.

Wieber, C., Jensen, L. Z., Vergeynst, L., Meire, L., Juul-Pedersen, T., Finster, K., and Šantl-Temkiv, T.: Terrestrial runoff is an important source of biological ice-nucleating particles in Arctic marine systems, Atmos. Chem. Phys., 25, 3327–3346, https://doi.org/10.5194/acp-25-3327-2025, 2025.

Wolf, K. K. E., Hoppe, C. J. M., Rehder, L., Schaum, E., John, U., and Rost, B.: Heatwave responses of Arctic phytoplankton communities are driven by combined impacts of warming and cooling, Sci. Adv., 10, eadl5904, https://doi.org/10.1126/sciadv.adl5904, 2024.

Wolf, M. J., Coe, A., Dove, L. A., Zawadowicz, M. A., Dooley, K., Biller, S. J., Zhang, Y., Chisholm, S. W., and Cziczo, D. J.: Investigating the Heterogeneous Ice Nucleation of Sea Spray Aerosols Using *Prochlorococcus* as a Model Source of Marine Organic Matter, Environ. Sci. Technol., 53, 1139–1149, https://doi.org/10.1021/acs.est.8b05150, 2019.

Wollesen de Jonge, R., Elm, J., Rosati, B., Christiansen, S., Hyttinen, N., Lüdemann, D., Bilde, M., and Roldin, P.: Secondary aerosol formation from dimethyl sulfide – improved mechanistic understanding based on smog chamber experiments and modelling, Atmos. Chem. Phys., 21, 9955–9976, https://doi.org/10.5194/acp-21-9955-2021, 2021.

Xu, W., Lambe, A., Silva, P., Hu, W., Onasch, T., Williams, L., Croteau, P., Zhang, X., Renbaum-Wolff, L., Fortner, E., Jimenez, J. L., Jayne, J., Worsnop, D., and Canagaratna, M.: Laboratory evaluation of species-dependent relative ionization efficiencies in the Aerodyne Aerosol Mass Spectrometer, Aerosol Sci. Technol., 52, 626–641, https://doi.org/10.1080/02786826.2018.1439570, 2018.

Xu, W., Ovadnevaite, J., Fossum, K. N., Lin, C., Huang, R.-J., O'Dowd, C., and Ceburnis, D.: Aerosol hygroscopicity and its link to chemical composition in the coastal atmosphere of Mace Head: marine and continental air masses, Atmos. Chem. Phys., 20, 3777–3791, https://doi.org/10.5194/acp-20-3777-2020, 2020.

Xu, W., Ovadnevaite, J., Fossum, K. N., Lin, C., Huang, R.-J., Ceburnis, D., and O'Dowd, C.: Sea spray as an obscured source for marine cloud nuclei, Nat. Geosci., 15, 282–286, https://doi.org/10.1038/s41561-022-00917-2, 2022.

Yan, S., Xu, G., Zhang, H., Wang, J., Xu, F., Gao, X., Zhang, J., Wu, J., and Yang, G.: Factors Controlling DMS Emission and Atmospheric Sulfate Aerosols in the Western Pacific Continental Sea, J. Geophys. Res.-Oceans, 129, e2024JC020886, https://doi.org/10.1029/2024JC020886, 2024.

Zamanillo, M., Ortega-Retuerta, E., Nunes, S., Rodríguez-Ros, P., Dall'Osto, M., Estrada, M., Montserrat Sala, M., and Simó, R.: Main drivers of transparent exopolymer particle distribution across the surface Atlantic Ocean, Biogeosciences, 16, 733–749, https://doi.org/10.5194/bg-16-733-2019, 2019.

Zhang, Y., Shen, F., Li, R., Li, M., Li, Z., Chen, S., and Sun, X.: AIGD-PFT: the first AI-driven global daily gap-free 4 km phytoplankton functional type data product from 1998 to 2023, Earth Syst. Sci. Data, 16, 4793–4816, https://doi.org/10.5194/essd-16-4793-2024, 2024a.

Zhang, Z., Liu, H., He, X., Zhang, Y., Wang, Y., Wang, Y., Liang, F., Li, Q., and Wu, G.: Satellite retrieval of oceanic particulate organic carbon: Towards an accurate and seamless dataset for the global ocean, Sci. Total Environ., 955, 176910, https://doi.org/10.1016/j.scitotenv.2024.176910, 2024b.

Zhao, Z., Gonsior, M., Schmitt-Kopplin, P., Zhan, Y., Zhang, R., Jiao, N., and Chen, F.: Microbial transformation of virus-induced dissolved organic matter from picocyanobacteria: coupling of bacterial diversity and DOM chemodiversity, ISME J., 13, 2551–2565, https://doi.org/10.1038/s41396-019-0449-1, 2019.

Zhou, C., Zhou, H., Holsen, T. M., Hopke, P. K., Edgerton, E. S., and Schwab, J. J.: Ambient Ammonia Concentrations Across New York State, J. Geophys. Res.-Atmos., 124, 8287–8302, https://doi.org/10.1029/2019JD030380, 2019.

Zou, H. and Hastie, T.: Regularization and Variable Selection Via the Elastic Net, J. Roy. Stat. Soc. B, 67, 301–320, https://doi.org/10.1111/j.1467-9868.2005.00503.x, 2005.